Snow albedo reduction in seasonal snow due to anthropogenic dust and carbonaceous aerosols across northern China

Xin Wang[1], Wei Pu[1], Yong Ren[1], Xuelei Zhang[2], Xueying Zhang[1], Jinsen Shi[1], Hongchun Jin[1],

Mingkai Dai[1], Quanliang Chen[3]

[1] Key Laboratory for Semi-Arid Climate Change of the Ministry of Education, College of Atmospheric Sciences, Lanzhou University, Lanzhou, 730000, China

[2] Key Laboratory of Wetland Ecology and Environment, Northeast Institute of Geography and Agroecology, Chinese Academy of Sciences, Changchun 130102, China

[3] College of Atmospheric Science, Chengdu University of Information Technology, and Plateau Atmospheric and Environment Laboratory of Sichuan Province, Chengdu 610225, China

Correspondence to: Xin Wang (wxin@lzu.edu.cn)

Atmospheric
Chemistry
and Physics

Open Access

Discussions

EGU

Abstract. A survey was performed to collect 92 seasonal snow samples across northern China in January 2014. The results show that mixing ratios of black carbon (BC), organic carbon (OC), and anthropogenic dust (AD) range from 60 to 4200 ng g^{-1}, 280 to 32000 ng g^{-1}, and 1300 to 5800 ng g^{-1} in surface snow, respectively. A relatively high

5   correlation (R^2=0.87, n=13) between OC and BC in surface snow is observed, indicating similar emission sources, and high OC/BC ratios suggest that biomass burning may be a major contributor at most snow sampling sites. In addition to the BC and AD parameters in the Snow, Ice, and Aerosol Radiation (SNICAR) model, the OC content in snow is considered an initial parameter for calculating snow albedo through

10   a new radiative transfer model (Spectral Albedo Model for Dirty Snow, or SAMDS). The spectral albedo of snow reduction caused by OC (20 μg g^{-1}) is up to a factor of 3 for a snow grain size of 800 μm compared to 100 μm. We find a larger difference in snow albedo levels between the model simulations and surface measurements for higher insoluble light-absorbing impurities (ILAPs) using the measured snow grain radii.

15   However, using the optical effective radii (R$_{eff}$), snow albedos modeled through both the SNICAR and SAMDS models are consistent with surface measurements, especially in the case of near-infrared wavelengths.

1   Introduction

Mineral dust (MD), black carbon (BC) and organic carbon (OC) are three insoluble light-absorbing particles (ILAPs) that play key roles in regional and global climate (IPCC, 2013; Jaffe et al., 1999). Anthropogenic dust (AD) is a major form of mineral dust. The AD content can influence air quality and human health through emission, transport, removal, and deposit processes (Aleksandropoulou et al., 2011; Chen et al., 2013; Huang et al., 2014, 2015a, 2015b; Kim et al., 2009; Li et al., 2009; Mahowald and Luo, 2003; Zhang et al., 2005, 2015). AD particles also act as cloud condensation nuclei that affect cloud formation (Coz et al., 2010; Givati and Rosenfeld, 2004; Rosenfeld et al., 2001) and deliver various trace nutrients to terrestrial and marine ecosystems (Acosta et al., 2011; Mahowald et al., 2005; Qiao et al., 2013). Ginoux et al. (2010) estimated that anthropogenic dust accounts for 25% of dust aerosols using observational data from MODIS Deep Blue satellite products combined with a land-use fraction dataset (Ginoux et al., 2010). Anthropogenic dust originates primarily from urban and regional sources, especially during the winter, and anthropogenic dust has already been enriched with heavy metals and other toxic elements (Kamani et al., 2015; Li et al., 2013; Wang et al., 2015; Zhang et al., 2013). Northeastern China and surrounding regions are generally regarded as industrial areas most affected by human activities. Because anthropogenic dust emissions from disturbed soils are not well constrained, we define mineral dust from areas disrupted by human activities, such as deforestation, overgrazing, agricultural and industrial activities, as anthropogenic dust (Aleksandropoulou et al., 2011; Tegen and Fung, 1995; Tegen et al., 2002, 2004; Thompson et al., 1988), which differs from natural mineral dust originating from desert regions (Che et al., 2011, 2013, 2015a; Goudie and Middleton, 2001; Li et al., 2012; Park and Park, 2014; Pu et al., 2015; Wallach and Fischer, 1970; Wang et al., 2008,

2010b). This assumption is consistent with the results of a recent study by Huang et al. (2015a), who found that anthropogenic dust contributions to regional emissions in eastern China are 91.8%, with India at 76.1% (e.g., Figure 10 in Huang et al., 2015a). This may be due to larger population densities, which are characterized by more intense

5   human activity in eastern China and India (Huang et al., 2015a; Wang et al., 2013a). Compared to AD, carbonaceous aerosols, such as BC and OC, generated from the incomplete combustion of fossil fuels and from biomass burning are also major anthropogenic pollutants. ILAPs deposited on snow have been found to shorten the snow cover season by decreasing the snow albedo and accelerating snow melt (Flanner

10   et al., 2007, 2009). Warren and Wiscombe (1980) found that a mixing ratio of 10 ng g^{-1} of soot in snow can reduce snow albedo levels by 1%. Light et al. (1998) determined that 150 ng g^{-1} of BC embedded in sea ice can reduce ice albedo levels by a maximum of 30% (Light et al., 1998). Among its main light-absorbing impurities, 1 ng g^{-1} of BC has approximately the same effect on the albedo at 500 nm as 50 ng g^{-1} of dust (Warren,

15   1982). Doherty et al. (2013) analyzed field measurements of vertical distributions of BC and other ILAPs in snow in the Arctic during the melt season and found significant melt amplification owing to an increased mixing ratio of BC by up to a factor of 5.

It is widely known that small snow albedo changes can have significant effects on global warming patterns, involving changes in snow morphology, sublimation, and melt

20   rates. Bond et al. (2013) estimated the industrial-era climate forcing of BC through all forcing mechanisms to be approximately +1.1 W m^{-2}, with 90% confidence limits of +0.17 to +2.1 W m^{-2}. This value includes the net effect of BC on radiation, clouds, and snow albedo, which have been found to heavily impact the earth's climate. Recent modeling studies have estimated regional and global radiative forcing caused by ILAPs

25   deposited on snow by reducing the surface albedo (Flanner, 2013; Flanner et al., 2007;

Atmospheric
Chemistry
and Physics
Discussions

Open Access

EGU

Hansen and Nazarenko, 2004; Jacobson, 2004; Koch et al., 2009; Qian et al., 2015; Zhao et al., 2014). Climate models have indicated that the reduction in surface albedo caused by BC leads to global warming and nearly global melting of snow and ice (Hansen and Nazarenko, 2004). Regional forcing by BC contamination in snow in

5 snow-covered regions, e.g., the Arctic and Himalayas (0.6 and 3.0 W m^{-2}, respectively), is comparable to carbon dioxide levels (1.5 W m^{-2}) in the atmosphere since the pre-industrial period (Flanner et al., 2007). The efficacy of radiative forcing due to BC deposited on snow has been estimated to be as high as 236% (Hansen et al., 2005).

Although AD is a less efficient absorber than BC and OC, in situ measurements of

10 seasonal snow across northern China and the Himalayas have shown high AD loadings (Guan et al., 2015; Kang et al., 2016; Wang et al., 2012, 2013a). In some regions, especially areas with thin and patchy snow cover and mountainous regions, soil dust significantly decreases the snow albedo, exceeding the influence of BC. However, models do not capture these potentially large sources of local dust in snowpack and

15 may overestimate BC forcing processes (Painter et al., 2007, 2010, 2012). Recently, several seasonal snow collection campaigns were performed across northern China, the Himalayas, North America, Greenland and the Arctic (Cong et al., 2015; Dang and Hegg, 2014; Doherty et al., 2010, 2014; Huang et al., 2011; Xu et al., 2009, 2012; Zhao et al., 2014). However, determining the effects of light-absorbing impurities on snow

20 albedo reduction continues to involve numerous challenges (Huang et al., 2011; Wang et al., 2013a; Ye et al., 2012; Zhang et al., 2013). We analyzed observed ILAPs in seasonal snow through a Chinese survey in 2014 following a snow campaign held in 2010 across northern China carried out by Huang et al. (2011). The area is seasonally covered with snow for approximately 3-6 months from late fall to early spring (Wang

25 et al., 2014). Our sampling sites were located across northeastern China and were

Atmospheric
Chemistry
and Physics
Discussions

positioned far from the northern boundaries of desert regions, such as the Gobi Desert in southern Mongolia and the Badain Jaran and Tengger Deserts in northwestern China (Li et al., 2009). Zhang et al. (2013), using a positive matrix factorization (PMF) receptor model, showed that industrial pollution sources are a major factor affecting

5   seasonal snow across northeastern China. Huang et al. (2015a) developed a new technique for distinguishing anthropogenic dust from natural dust based on Cloud-Aerosol Lidar and Infrared Pathfinder Satellite Observation (CALIPSO) dust and planetary boundary layer (PBL) height retrievals along with a land-use dataset. The authors found that the annual mean contribution of anthropogenic dust in eastern China

10   is approximately 91.8% owing to recent urbanization and human activity (Huang et al., 2015a). In this paper, we explore the climatic effects of ILAPs (including BC, OC, and AD) on seasonal snow across northeastern China, which are highly correlated with industrial pollution resulting from human activity. Therefore, ILAPs in seasonal snow are examined during a snow campaign, and the snow albedo is measured using an HR-

15   1024 field spectroradiometer and simulated using two radiative transfer models (i.e., SNICAR and SAMDS).

2   Experimental procedures

2.1   Snow field campaign

In 2014, there was less snowfall in January than in previous years (e.g., 2010), and only
20   92 snow samples at 13 sites were collected. Samples from sites 90-93 were collected from grassland and cropland areas in Inner Mongolia. Sites 94-98 and sites 99-102 were located in the Heilongjiang and Jilin provinces, respectively, which are the most heavily polluted areas in northern China during winter. The snow sampling routes were similar to those used in the previous survey conducted in 2010 across northern China (Huang

et al., 2011). To prevent contamination, the sampling sites were positioned 50 km from cities and at least 1 km upwind of approach roads or railways; the only exception was site 101, which was positioned downwind and close to villages. We gathered snow samples every 5 cm from the surface to the bottom unless a particularly dusty or

5   polluted layer was present. Snow grain sizes were measured by visual inspection on millimeter-gridded sheets viewed through a magnifying glass. The snow samples were kept frozen until the filtration process was initiated. In a temporary lab based in a hotel, we quickly melted the snow samples in a microwave, let them settle for 3-5 minutes, and then filtered the resulting water samples through a 0.4-µm nuclepore filter to extract

10   particulates.

2.2   Chemical speciation

The chemical analysis of snow samples from the 2014 Chinese survey was described by Wang et al. (2015), and it was similar to the analysis applied for snow samples described by Hegg et al. (2009, 2010). Briefly, major ions (SO_4^{2-}, NO_3^-, Cl^-, Na^+, K^+,

15   and NH_4^+) were analyzed with an ion chromatograph (Dionex, Sunnyvale, CA), and trace elements were measured by inductively coupled plasma mass spectrometry (ICP-MS). These analytical procedures have been described elsewhere (Yesubabu et al., 2014). Previous studies have revealed considerable variations in iron (Fe) of 2-5% in dust (Lafon et al., 2006), although Al is more stable than Fe in the earth's crust. Hence,

20   we retrieved the mass concentration of minerals via the Al concentration assuming a fraction of 7% when estimating the dust levels (Arhami et al., 2006; Lorenz et al., 2006; Zhang et al., 2003). Sea salt was estimated following the method presented in Pio et al. (2007):

$$\text{Sea salt} = Na_{Ss}^+ + Cl^- + 0.12Na_{Ss}^+ + 0.038Na_{Ss}^+ + 0.038Na_{Ss}^+ + 0.25Na_{Ss}^+, \qquad (1)$$

Atmospheric
Chemistry
and Physics
Discussions

Open Access
EGU

where Na_{Ss} was calculated using the following formula (Hsu et al., 2009):

$$Na_{Ss} = Na_{Total} - Al \times (Na/Al)_{Crust}. \tag{2}$$

Following Hsu et al. (2009), the contribution of $K^{+}_{Biosmoke}$ was determined using the following equations:

5
$$K^{+}_{Biosmoke} = K_{Total} - K_{Dust} - K_{Ss}, \tag{3}$$

$$K_{Dust} = Al \times (K/Al)_{Crust}, \tag{4}$$

$$Na_{Ss} = Na_{Total} - Al \times (Na/Al)_{Crust}, \tag{5}$$

$$K_{Ss} = Na_{Ss} \times 0.038. \tag{6}$$

Equations (4), (5), and (6) were derived from Hsu et al. (2009) and Pio et al. (2007).

10 **2.3   Spectrophotometric analysis**

Assuming that iron originated from mineral dust in seasonal snow, we measured the mixing ratios of BC and OC using an integrating sphere/integrating sandwich spectrophotometer (ISSW), which was first described by Grenfell et al. (2011) and used by Doherty et al. (2010, 2014) and Wang et al. (2013a) to measure mixing ratios of BC

15 and OC. The equivalent BC (C^{equiv}_{BC}), maximum BC (C^{max}_{BC}), estimated BC (C^{est}_{BC}), fraction of light absorption by non-BC ILAPs (f^{est}_{non-BC}), and absorption Ångstrom exponent (Å_{tot}) were described by Doherty et al. (2010). Previous studies have concluded that light-absorbing particles are primarily derived from BC, OC, and iron (Fe). The mass loadings of BC and OC were calculated using the following equation:

20
$$\tau_{tot}(\lambda) = \beta_{BC}(\lambda) \times L_{BC} + \beta_{OC}(\lambda) \times L_{OC} + \beta_{Fe}(\lambda) \times L_{Fe}. \tag{7}$$

Here, L_{BC} and L_{OC} can be determined from this equation assuming that the mass absorption efficiencies (β) for BC, OC, and Fe are 6.3, 0.3, and 0.9 $m^2\,g^{-1}$, respectively,

Atmospheric
Chemistry
and Physics
Discussions

at 550 nm and that the absorption Ångstrom exponents for BC, OC and Fe are 1.1, 6, and 3, respectively (e.g., Equations (2) and (3) in Wang et al., 2013a).

2.4   Aerosol optical depth and snow albedo measurements

We used a portable and reliable Microtops Π Sun photometer at wavelengths of 340,

5   440, 675, 870, and 936 nm instead of the CE318 sun tracking photometer (Holben et al., 2006) to measure the in situ aerosol optical depth (AOD). Morys et al. (2001) provided a general description of the Microtops Π Sun photometer's design, calibration, and performance. The Microtops Π Sun photometer has been widely used in recent years (de Mourgues et al., 1970; Porter et al., 2001; Zawadzka et al., 2014) and is

10   recognized as a very useful tool for validating aerosol retrievals from satellite sensors. A Microtops Π Sun photometer was calibrated following the methods presented by Morys et al. (2001) and Ichoku et al. (2002b). To better understand the background weather conditions in the local atmosphere, a Microtops Π Sun photometer was used during the 2014 Chinese survey. AOD measurements were collected in cloud-free

15   conditions between 11:00 am and 1:00 pm (Beijing local time) to prevent the effects of optical distortions due to large solar zenith angles. We used the Moderate Resolution Imaging Spectroradiometer (MODIS) on the Aqua and Terra satellites to retrieve the AOD and fire spot datasets (Kaufman et al., 1997; Zhang et al., 2013; Zhao et al., 2014). The retrieved MODIS AOD is reliable and accurate when applied to three visible

20   channels over vegetated land and ocean surfaces (Chu et al., 2002; Ichoku et al., 2002a; Remer et al., 2002). Fire locations are based on data provided by the MODIS FIRMS system from October to January.

Spectroradiometers have been used to measure the surface spectral albedo (Kotthaus et al., 2014; Wright et al., 2014; Wuttke et al., 2006). In the 2014 Chinese survey, snow

Atmospheric
Chemistry
and Physics
Discussions

Open Access

EGU

albedo measurements were obtained using a HR-1024 field spectroradiometer (SVC,

Spectra Vista Corporation, Poughkeepsie, NY, USA). This instrument has a spectral

range of 350-2500 nm with resolutions of 3.5 nm (350–1000 nm), 9.5 nm (1000–1850

nm), and 6.5 nm (1850–2500 nm). According to previously described procedures, we

5   measured the snow albedo 1 m above the ground (Carmagnola et al., 2013). A standard

"white" reflectance panel with a VIS–SWIR broadband albedo of 0.98 (P_λ) was used to

measure the reflectance spectra along with the target. The reflectance spectra of surface

snow (R_s) and the standard panel (R_p) were measured at least ten times. Then, the snow

albedo (α) was calculated as follows:

10          $\alpha = (R_s/R_p) \times P_\lambda.$ (8)

Further information on HR-1024 field spectroradiometer use and on the calibration

procedure can be found in Wright et al. (2014).

2.5   Model simulations

BC and dust sensitivity effects on the snow albedo simulated by the Snow, Ice, and

15   Aerosol Radiation (SNICAR) model have been validated through recent simulations

and field measurements (Flanner et al., 2007, 2009; Qian et al., 2014; Zhao et al., 2014).

We used the offline SNICAR model to simulate the reduction in surface snow albedo

resulting from ILAP contamination (Flanner et al., 2007), and we compared the results

with our spectroradiometer surface measurements. The SNICAR model calculates the

20   snow albedo as the ratio of the upward and downward solar flux at the snow surface.

The measured parameters, including the snow grain radius, snow density, snow

thickness, solar zenith angle, and mixing ratios of BC and AD, were used to run the

SNICAR model under clear sky conditions. The visible and near-infrared albedos of

the underlying ground were 0.2 and 0.4, respectively, as derived from MODIS remote

Atmospheric
Chemistry
and Physics
Discussions

sensing. The mass absorption cross section (MAC) was assumed to be 7.5 m^2 g^{-1} at 550 nm.

The Spectral Albedo Model for Dirty Snow (SAMDS) for calculating spectral snow albedo as a function of the snow grain radius, the mixing ratios of ILAPs (BC, AD, and

5   OC), and mass absorption efficiencies of impurities was used and is based on asymptotic radiative transfer theory. This model explicitly considers (i) mixing states between impurities and snow grains, (ii) the irregular morphology of snow grains and aerosol particles, (iii) specific mineral compositions and size distributions of dust in snow, (iv) aging processes of snow grains and soot aggregates, and (v) multilayers for

10   studying vertical distributions of snow grains and impurities.

Briefly, the surface albedo can be calculated using the following asymptotic approximate analytical solution derived from radiative transfer theory (Kokhanovsk and Zege, 2004; Rozenberg, 1962; Zege et al., 1991):

$$R_d(\lambda) = \exp(-4S(\lambda)\mu(v_0)). \tag{9}$$

15   Here, $R_d(\lambda)$ is the plane albedo, v_0 is the solar zenith angle, and $u(v_0)$ can be parameterized following Kokhanovsky and Zege (2004):

$$\mu(v_0) = \frac{3}{7}(1+2\cos v_0), \tag{10}$$

where λ is the wavelength, $S(\lambda)$ is the similarity parameter, and

$$S(\lambda) = \sqrt{\frac{\sigma_{abs}}{3\sigma_{ext}(1-g)}}. \tag{11}$$

20   Here, σ_{abs} and σ_{ext} are the absorption and extinction coefficients, respectively, and g is the asymmetry parameter (the average cosine of the phase function of the medium).

According to Equations (18) and (25) in Kokhanovsky and Zege (2004), the extinction coefficients of particles can be expressed as follows:

$$\sigma_{ext} = \frac{l_{tr}}{1-g} = \frac{3C_v}{2r_{ef}},$$ (12)

where l_{tr} is the photon transport path length, C_v is the volumetric snow particle concentration, and r_{ef} is the effective grain size, which is equal to the radius of the volume-to-surface equivalent sphere: $r_{ef} = \frac{3\overline{V}}{4\overline{A}}$, where $\overline{V}$ and $\overline{A}$ are the average volume and average cross-sectional (geometric shadow) area of snow grains, respectively.

The absorption coefficient σ_{abs} in Equation (11) for arbitrarily shaped and weakly absorbing large grains is proportional to the volume concentration (Kokhanovsky and Zege, 2004):

$$\sigma_{abs} = B \cdot \frac{4\pi k(\lambda)}{\lambda} \cdot C_v,$$ (13)

where $k(\lambda)$ is the imaginary component of the complex refractive index for ice, and B is a factor that is only dependent on the particle shape.

The total absorption coefficient, σ_{abs}, can be derived from the absorption by snow, S_{abs}^{snow}, and the absorption by light-absorbing impurities, S_{abs}^{dust}, S_{abs}^{BC}, and S_{abs}^{OC}:

$$\sigma_{abs} = \sigma_{abs}^{snow} + \sigma_{abs}^{dust} + \sigma_{abs}^{BC} + \sigma_{abs}^{OC}.$$ (14)

The hemispherical reflectance with a zenith angle v_0 can be expressed as follows:

$$R_d(\lambda) = \exp\left(-4\cdot\sqrt{\frac{4B}{9(1-g)}}\cdot\sqrt{\frac{2\pi\cdot r_{ef}}{\lambda}\cdot k(\lambda)+\frac{\rho_{ice}\cdot 2r_{ef}}{9(1-g)}\cdot MAC_{abs}^{dust}\cdot C_{dust}^{*}+\frac{\rho_{ice}\cdot 2r_{ef}}{9(1-g)}\cdot MAC_{abs}^{BC}\cdot C_{BC}^{*}+\frac{\rho_{ice}\cdot 2r_{ef}}{9(1-g)}\cdot MAC_{abs}^{OC}\cdot C_{OC}^{*}\cdot\frac{3}{7}(1+2\cos v_0)}\right)$$

$$\exp\left(-\sqrt{94.746\cdot\frac{r_{ef}}{\lambda}\cdot k(\lambda)+5.163\cdot r_{ef}\cdot(MAC_{abs}^{dust}\cdot C_{dust}^{*}+MAC_{abs}^{BC}\cdot C_{BC}^{*}+MAC_{abs}^{OC}\cdot C_{OC}^{*})\cdot(1+2\cos v_0)}\right), \quad \text{for spherical grains;}$$

$$= \exp\left(-4.95\cdot\sqrt{\frac{\pi\cdot r_{ef}\cdot(k(\lambda)+\alpha\cdot C_{dust}^{*}+\beta\cdot C_{BC}^{*}+\chi\cdot C_{OC}^{*})}{\lambda}\cdot(1+2\cos v_0)}\right), \quad \text{for hexagonal grains;} \qquad (15)$$

$$\exp\left(-4.38\cdot\sqrt{\frac{\pi\cdot r_{ef}\cdot(k(\lambda)+\alpha\cdot C_{dust}^{*}+\beta\cdot C_{BC}^{*}+\chi\cdot C_{OC}^{*})}{\lambda}\cdot(1+2\cos v_0)}\right), \quad \text{for fractal grains.}$$

5

13

A detailed description of asymptotic analytical radiative transfer theory for snowpack

was presented by Zhang et al. (2016). Previous studies have also shown that the spectral

snow albedo is more sensitive to snow grain size and light conditions than BC

contamination and snow depths at near-infrared wavelengths (Warren, 1982). Therefore,

5   the snow grain optical effective radius was retrieved based on the spectral albedo

measured at $\lambda=1.3$ µm (Table 4), where snow grain size dominates the snow albedo

variations and the effects of light-absorbing particles at this wavelength are negligible

(Warren and Wiscombe, 1980).

3   Results

10   **3.1   The spatial distribution of AOD**

The AOD is a major optical parameter for aerosol particles and a key factor affecting

global climate (Holben et al., 1991, 2001; Smith et al., 2014; Srivastava and Bhardwaj,

2014). For most of the snow samples collected in the afternoon at the Aqua-MODIS

(13:30 LT) overpass time, the averaged spatial AOD distribution was derived from the

15   Aqua-MODIS satellite "Aerosol" product during the sampling period across northern

China. The AOD spatial distribution over northern China is shown in Figure 1 for the

period from October to January. The average AOD in the studied area ranged from 0.1

to 1.0 and exhibited strong spatial inhomogeneity. The largest AODs (up to

approximately 1.0) retrieved from the MODIS satellite were associated with

20   anthropogenic pollution over northeastern China during the 2014 sampling period.

These large values, which exceeded 0.6, were related to local air pollution from

industrial areas (Che et al., 2015b; Wang et al., 2010a). In contrast, the MODIS-Aqua

results indicate that the smallest AODs (as low as 0.1) at 550 nm were found over the

Gobi Desert in Inner Mongolia and were related to strong winter winds. Similar patterns

in the retrieved MODIS AOD were found by Zhao et al. (2014) and Zhang et al. (2013).
Although previous studies have indicated that AODs in northeastern China are among
the highest in East Asia (Ax et al., 1970; Bi et al., 2014; Che et al., 2009; Routray et al.,
2013; Wang et al., 2013b; Xia et al., 2005, 2007), field experiments of aerosol optical

5   properties across northeastern China have been limited. To evaluate the accuracy of the
AODs, in situ AOD measurements were collected during the snow sampling period in
January 2014. The in situ AOD measurements were generally consistent with the spatial
AOD distribution retrieved from MODIS across northern China, although the retrieved
AOD was slightly higher than that retrieved from the in situ measurements in the study

10   area. In Inner Mongolia, the average AOD was less than 0.25 for sites 1 to 6 under clear
conditions. We found large variations of 40-50% in the same area in the 1-hour
measurements collected from sites 6a and 6b; these variations were correlated with
regional biomass burning processes. However, AODs exceeded 0.3 at sites 9 and 12,
which were significantly influenced by anthropogenic air pollution from industrial

15   areas across northern China. MODIS active fires are often spatially distributed over
northeastern China and mainly result from human activities during colder seasons.

3.2   Sampling statistics

C_{BC}^{est}, C_{BC}^{max}, C_{BC}^{equiv}, f_{nonBC}^{est}, $Å_{tot}$ and snow parameters, such as snow depth, snow
density, snow grain radius, and snow temperature, are given in Table 1 and Figure 3 for

20   each snow layer following Wang et al. (2013a). Average C_{BC}^{est}, C_{BC}^{max}, and C_{BC}^{equiv}
values were calculated using "left" and "right" samples for each layer. The snow cover
was thin and patchy in Inner Mongolia, and the average snow depth was less than 10
cm from sites 90, 91, 93, and 94, which slightly higher values near the northern border
of China, ranging from 13 to 20 cm at sites 95-97. The maximum snow depth of 46 cm

Atmospheric
Chemistry
and Physics
Discussions

at site 102 was found in a forest near the Changbai Mountains, averaging 27 cm and
varying from 13 to 46 cm at sites 98 to 102. Because less snow fell during the 2014
snow survey period, the surface snow grain radius varied considerably from 0.07 to 1.3
mm. The snow grain size increased with the snow depth from the surface to the bottom

5   and was larger than that recorded in previous studies because of snow melting by solar
radiation and the ILAPs (Hadley and Kirchstetter, 2012; Motoyoshi et al., 2005; Painter
et al., 2013; Pedersen et al., 2015). The snow density exhibited little geographical
variation across northern China at 0.13 to 0.38 g cm^{-3}. High snow densities result from
melting or snow aging. Similar snow densities have been found in the Xinjiang region

10   in northern China (Ye et al., 2012). Å$_{tot}$ ranged from 2.1 to 4.8. A higher Å$_{tot}$ is a good
indicator of soil dust, which is primarily driven by the composition of mineral or soil
dust. In contrast, a lower Å$_{tot}$ of 0.8-1.2 indicates that light-absorbing particulates in the
snow are dominated by BC (Bergstrom et al., 2002; Bond et al., 1999).

To better understand the BC distribution in seasonal snow across northern China, an

15   interannual comparison of the BC content in the surface and average snow measured
during the 2010 and 2014 Chinese surveys was performed, and the results are shown in
Figure 4 and Table 2. The spatial distributions of BC in the surface and average snow
measured using an ISSW spectrophotometer during the 2014 survey generally ranged
from 53 to 3651 ng g^{-1} and 62 to 1635 ng g^{-1}, respectively. These variations were very

20   similar to those of the previous snow campaign, as shown in Figure 4 (Wang et al.,
2013a), although they were much higher than those in the Xinjiang region of
northwestern China (Ye et al., 2012), along the southern edge of the Tibetan Plateau
(Cong et al., 2015), and in North America (Doherty et al., 2014). In the 2014 Chinese
survey, we only collected one layer of snow samples from central Inner Mongolia, and

25   the BC mixing ratio was 334 ng g^{-1} in aged snow. Along the northern Chinese border

at sites 91-95, BC contamination in the cleanest snow ranged from 27 to 260 ng g^{-1}; only a few values exceeded 200 ng g^{-1}. The f_{nonBC}^{est} value varied remarkably from 29 to 78%, although BC was still a major absorber in this region. Heavily polluted sites were located in industrial regions across northeastern China (sites 99-102). The surface

5   snow BC in this region ranged from 508 to 3651 ng g^{-1}, and the highest BC in the sub-surface layer of the four sites was 2882 ng g^{-1}. In addition, the fraction of total particulate solar absorption due to f_{nonBC}^{est} was typically 35-74%, indicating that light absorption in snow is mainly attributable to OC and AD from human activity.

Figure 5 compares the BC mixing ratio measured via the ISSW method with the

10   calculations. Ideally, the BC content calculated using Equation (7) should be equal to that measured via the ISSW method. The two results agreed very well (R^2=0.99), indicating that Equation (7) worked well for this measurement. Thus, the BC content measured via the ISSW method was found to be reasonable and reliable. To compare with the mixing ratio of OC calculated from Equation (7), we used the calculated BC

15   mixing ratios listed in Figures 6-8 and Table 3 in the following sections.

3.3   Emission factors

Typically, chemical components in seasonal snow originate from different emission sources. For example, OC and BC are emitted from the incomplete combustion of fossil fuels and biofuels. K$^+$ is a good tracer of biomass burning (Cachier et al., 1995), whereas

20   NO$_3^-$ and SO$_4^{2-}$ originate primarily from diesel oil and gasoline combustion and from coal burning with sulfur. NH$_4^+$ is an important indicator of fertilizer used in agricultural processes. OC/BC ratios are used to represent possible emission sources of biomass burning (Bond et al., 2013; Cao et al., 2007; Cong et al., 2015; Novakov et al., 2005). The OC/BC ratio in the sampled surface snow ranged from 1.4 to 17.6 (Figure 6); a

Atmospheric
Chemistry
and Physics
Discussions

Open Access

very high OC/BC ratio (17.6) was found at site 90, suggesting that biomass burning

may have been a major contributor of OC through photochemical reactions during the

2014 Chinese survey. A relatively high correlation (R^2=0.87, n=13) was observed

between OC and BC, indicating similar emission sources at all sampling sites except

5 for those in central Inner Mongolia, as shown in Figure 6a. These results are consistent

with those of previous studies (Ming et al., 2010). The strong correlations between

NH_4^+/SO_4^{2-} and NH_4^+/NO_3^- shown in Figures 6b and 6c (R^2=0.91 and R^2=0.94,

respectively; n=12) suggest that fine particles characterized as $(NH_4)_2SO_4$ and NH_4NO_3

were derived from more intense agricultural and human activities occurring near

10 farmland areas (Ianniello et al., 2011). It is widely accepted that crustal Al originates

from mineral or soil dust (Wedepohl, 1995). Therefore, the weak correlation between

K^+ and Al could be explained by different emission sources of K^+ and Al (Figure 6d)

often attributed to biomass burning and mineral or soil dust, respectively, in local or

remote regions. Sampling site 101 (red dot in Figure 6d) is positioned very close to a

15 village. As a result, we found a much higher K^+ than Al value owing to high biomass

burning via human activity in winter.

3.4   Mass contributions of chemical components

The land-cover types (Figure 7) were obtained from the Collection 5.1 MODIS global

land-cover type product (MCD12C1) at a 0.05° spatial resolution and included 17

20 different surface vegetation types (Friedl et al., 2010; Loveland and Belward, 1997).

The sampling areas were located in grasslands, croplands, and urban and built-up

regions across northern China that are likely influenced by human activity (Huang et

al., 2015a). According to Table 3 and Figure 7, the NH_4^+ concentrations emitted from

agricultural sources at all sites accounted for less than 2.8% because the sites were

18

positioned 50 km from cities. However, large fractions of both SO_4^{2-} and NO_3^- were observed, varying from 14.8 to 42.8% at all sites, with the highest fraction of 24.2-42.8% found in industrial areas. These results show that SO_4^{2-} and NO_3^- made the greatest contributions to the total chemical concentration in the surface snow and are

5   significant anthropogenic sources of fossil-fuel combustion in heavy industrial areas. More specifically, the largest AD contribution ranged from 35.3 to 46% at sites 91 to 95 owing to strong winds during winter; the AD fractions were only 5.7 to 31% at the other sites. Fractions of BC and OC were similar to those above, showing that biomass burning was a major source during winter in the sampling region. Zhang et al. (2013)

10   showed that OC and BC fractions vary more widely in the winter than other seasons owing to industrial activity in China. Sulfate peaks were found in summer (15.4%), whereas nitrate peaks were observed in spring (11.1%). Potassium ($K^+_{biosmoke}$) was found to be a good tracer of biomass burning, ranging from 1.3 to 5.1% along the northern Chinese border compared to lower values found at lower latitudes (1.5-2.3%),

15   and it exhibited much higher contributions in Inner Mongolia and along the northern Chinese border owing to increased emissions from cooking, open fires, and agricultural activities. The fraction of sea salt aerosol was found to range from 6.3 to 20.9%. Wang et al. (2015) showed that higher Cl^-/Na^+ ratios in seasonal snow found in the 2014 Chinese survey were 1 - 2 times greater than those of seawater, implying that they

20   constituted a significant source of anthropogenic Cl^- (Wang et al., 2015).

3.5   BC, OC and AD contributions to light absorption

As described by Wang et al. (2013a), light absorption by ILAPs can be determined from ISSW measurements combined with a chemical analysis of iron concentrations by assuming that the light absorption of dust is dominated by iron (Fe); however, iron can

also originate from industrial emissions. Doherty et al. (2014) used a similar method to distinguish between contributions of light-absorbing impurities in snow in central North America. Although heavy AD loading was observed in the study region, the fraction of light absorption due to AD (assumed to exist as goethite) was generally less than 10%

5   across northeastern China (Figure 8), which was much smaller than that observed in the Qilian Mountains (e.g., Figure 11 of Wang et al., 2013a). Light absorption was mainly dominated by BC and OC in snow in January 2014. By contrast, the fraction of light absorption due to BC varied from 48.3 to 88.3% at all sites, with only one site dominated by OC (site 90 in central Inner Mongolia). Compared to the light absorption

10   patterns in the Qilian Mountains, iron played a less significant role in particulate light absorption in snow across the northeastern China sampling area.

3.6   Comparisons between the observed and modeled snow albedo

Snow albedo reduction due to BC has been examined in previous studies (Brandt et al., 2011; Hadley and Kirchstetter, 2012; Yasunari et al., 2010). However, few observations

15   of the BC, OC, and AD mixing effects on snow albedo reduction in seasonal snow at middle latitudes exist. In this study, we measured the snow albedo at six sites under clear conditions. A comparison of the snow albedos derived from the SNICAR and SAMDS models is presented in Figure 9. Spectral snow albedos measured in our experiments and simulated through the SNICAR and SAMDS models are shown in

20   Figure 11. We ran the models at a solar zenith angle of 60 °C, which is consistent with our experimental method for measuring albedo and with light-absorbing impurities across northern China. Mixing ratios of BC, OC, and dust were chosen to exhibit the following ranges: 0-5 μg g^{-1}, 0-30 μg g^{-1}, and 0-6 μg g^{-1}, respectively, encompassing the values measured in snow surfaces across northern China in previous research

Atmospheric
Chemistry
and Physics
Discussions

(Warren and Wiscombe, 1980) and in this study. The BC MAC used in this study was

7.5 m^2 g^{-1} at 550 nm, which was assumed in the most recent climate assessment and is

appropriate for freshly emitted BC (Warren, 1982; Bond and Bergstrom, 2006; Bond et

al., 2013). The visible and near-infrared albedos of underlying ground surfaces were

5   0.2 and 0.4, respectively, according to the MODIS data. The spectral albedos of pure

snow derived from the SNICAR (dash line) and SAMDS (solid line) models agreed

well. However, there was a slight tendency for the SNICAR model values to become

lower than SAMDS model values when BC and dust mixing ratios range from 1 to 5

μg g^{-1} and 4 to 6 μg g^{-1}, respectively. The 1.5-2.5% deviation between the SNICAR and

10   SAMDS modeled snow albedos at 550 nm for higher BC mixing ratios indicates that

albedo reduction by light-absorbing impurities in the SNICAR model was greater than

that of the SAMDS model. More notably, snow albedos decreased significantly within

the UV-visible wavelength, especially for the higher OC (dotted lines) contents in

Figure 9. This may be attributed to the fact that OC strongly absorbs UV-visible

15   radiation and masks BC absorption for high AAE of OC, which decreases remarkably

with increasing wavelengths (Warren and Wiscombe, 1980).

As is shown in Figure 10, we also estimated the reduction in the spectrally weighted

snow albedo for different R_{eff} values using the SNICAR and SAMDS models. Higher

degrees of snow albedo reduction by both BC and dust-contaminated snow were

20   generally found for larger snow grains (Figure 10a-b). For example, snow albedo

reduction attributable to 1000 ng g^{-1}, 1 μg g^{-1}, and 10 μg g^{-1} for BC, dust, and OC,

respectively, was 37%, 41%, and 38% greater in 200 μm snow (0.081, 0.0019, and

0.047) than that in 100 μm snow (0.059, 0.0013, and 0.034). Both the SNICAR and

SAMDS models indicated that the snow albedo is more sensitive to BC, especially

25   during lower ILAP periods. For example, 200 ng g^{-1} of BC decreased the snow albedo

by 3.4% for an optical effective radius of 200 µm, which is much larger than the snow

albedo reduction of 2 µg g^{-1} for dust and OC at an optical effective radius 200 µm. As

Hadley and Kirchstetter (2012) noted, compared with pure 55 µm snow, 300 ng g^{-1} of

BC contamination and growth to 110 µm causes a net albedo reduction of 0.11 (from

5   0.82 to 0.71), causing snow to absorb 61% more solar energy (Hadley and Kirchstetter,

2012). Previous studies have also indicated that the mixing ratio of BC (10-100 ng g^{-1})

in snow may decrease its albedo by 1-5% depending on its aging process (Warren and

Wiscombe, 1980; Hansen and Nazarenko, 2004).

Figure 11 compares snow albedo values under clear sky conditions collected through

10   surface measurements and the SNICAR and SAMDS models based on Toon et al.'s

(1989) two-stream radiative transfer solution. The model input parameters are listed in

Tables 1 and 4. The MAC of BC used in the ISSW was 6.3 m^2 g^{-1} at 550 nm, although

a value of 7.5 was used in the NICAR and SAMDS models. Thus, the mixing ratio of

BC was corrected by dividing it by 1.19 when BC was used as the input parameter to

15   the snow albedo models (Wang et al., 2013a). The snow albedos measured at 550 nm

varied considerably from 0.99 to 0.61 owing to different mixing ratios of ILAPs and

snow parameters, such as snow grain size. The snow albedos predicted by the SNICAR

and SAMDS models agreed well at each site based on the same input parameters. The

snow albedos of the SNICAR and SAMDS models retrieved from measured snow grain

20   sizes complemented the surface measurements for lower mixing ratios of BC, OC, and

AD. The highest BC mixing ratios were 1461 and 3651 ng g^{-1} at sites 98 and 101,

respectively, across industrial regions, with median values found in integrated layers of

264 and 1635 ng g^{-1}, respectively. The OC and dust mixing ratios were as high as 13.3

µg g^{-1} and 32 µg g^{-1} in this region. The higher AD mixing ratios are consistent with

25   previous studies conducted by Zhang et al. (2013) and Huang et al. (2015a), who

Atmospheric
Chemistry
and Physics
Discussions

indicated that AD is highly correlated with anthropogenic air pollution originating from human activity across northeastern China. Thus, we found a larger difference in snow albedo of up to 0.2 at higher BC, OC, and AD contents between the surface measurements and the modeled albedos for the measured snow grain sizes at sites 91,

5 98, and 101. When the reduction in albedo caused by light-absorbing impurities at the inferred wavelength by measured snow grain size was not accounted for, we also calculated the snow albedos from the SNICAR and SAMDS models using the optical effective size shown in Figure 11 (blue and red shaded bands), and these values were consistent with the surface measurements (gray shaded bands), especially at near-

10 infrared wavelengths. This may be attributed to the fact that the optical effective size at these three sampling sites was much larger than the measured grain size, indicating that the radiative perturbation of light-absorbing impurities was amplified with snow grain optical effective size. As indicated in Figure 11, BC, OC, and AD are three types of ILAPs found in snow that can reduce spectral snow albedo levels. Reduced snow albedo

15 due to ILAPs in our measurements were generally comparable to the modeled effects found in the commonly used SNICAR and SAMDS models (Flanner et al., 2007; Zhang et al., 2016). Therefore, 100-500 ng g^{-1} of BC can lower the snow albedo by 2-6% relative to pure snow with a snow grain size of 200 μm according to our snow field campaign, and AD was found to be a weak absorber owing to its lower AD MAC,

20 supporting previous observations made by Warren and Wiscombe (1980). The OC MAC was also lower and comparable to that of the AD. A clear decreasing trend in the surface snow albedo owing to the high ambient mixing ratios of OC from Inner Mongolia to northeastern China was found. The radiative transfer modeling results presented by Zhang et al. (2016) and measurement results of this study show that the

25 spectral albedo of snow reduction caused OC levels (above 20 μg g^{-1}) to increase by a

Atmospheric
Chemistry
and Physics
Discussions

factor of 3 for a snow grain size of 800 μm compared to 100 μm.

4   Discussion and conclusions

In this study, a Chinese survey was performed in January 2014. We collected 92 snow samples from 13 sites across northern China. Much less snow had fallen than in previous years; as a result, most of the surface snow samples were collected as aged snow, and snow grain sizes were much larger owing to solar radiation absorbed by ILAPs as a result of settlement processes. Although we selected study locations in remote regions located at least 50 km from cities, higher AODs measured using a sun photometer and remote sensing devices showed that heavily polluted areas remain in industrial regions across northern China. The estimated BC mixing ratios measured through the 2014 survey via the ISSW spectrophotometer in surface and average integrated snow of 53 to 3651 and 62 to 1635 ng g^{-1}, respectively, were much larger than those of previous snow field campaigns. The non-BC fraction showed that most of the ILAPs in seasonal snow were dominated by OC and AD. Owing to BC and OC mass absorption efficiencies of 6.3 and 0.3 m^2 g^{-1}, respectively, at 550 nm, light absorption was still dominated by BC and OC in seasonal snow during the entire campaign. AD contributions in snow to light absorption amounted to less than 10%. The large OC/BC ratios and correlation coefficients indicated that these contributions were mainly derived from common sources (e.g., biomass burning). Similarly, NH$_4^+$ was attributed to intense agricultural activity compared to industrial emissions of SO$_4^{2-}$ and NO$_3^-$.

The fraction of the AD mixing ratios was larger at high latitudes than at low latitudes owing to strong winds transporting snow. OC emitted from biomass burning and SO$_4^{2-}$ and NO$_3^-$ generated from fossil fuels and biofuels also played key roles in the mixing

24

ratios of chemical components in seasonal snow. Finally, a comparison between measured and simulated snow albedos was conducted. The snow albedos measured from a spectroradiometer and simulated using the SNICAR and SAMDS models agreed with the lower mixing ratios of BC, OC, and AD. Based on the snow grain optical

5   effective size, we found good agreement between surface measurements and radiative transfer models. Therefore, the snow grain optical effective size is preferred when measurements on snow grain size are available at the near-infrared wavelength. Although the MAC of OC was much lower than that of BC, we found that OC was a major absorber in snow owing to its high mixing ratio of OC from human activities

10   occurring across northeastern China. Moreover, 5000 ng g^{-1} of OC was found to reduce the snow albedo by 1.5%-5% depending on the snow grain size and aging period. Therefore, we suggest that the mixing ratio of OC be added as an input parameter to the SNICAR model for determining snow albedos.

15

20

Atmospheric
Chemistry
and Physics
Discussions

Atmospheric
Chemistry
and Physics
Discussions

Table 1. Statistics on seasonal snow variables measured using an ISSW in the study sites.

Site	Layer	Latitude N	Longitude E	Site average snow depth (cm)	Sample depth (cm) Top	Sample depth (cm) Bottom	Temperature (°C)	Snow density (g cm^{-3})	Snow grain radius (mm)	C_{BC}^{equiv} (ng g^{-1})	C_{BC}^{max} (ng g^{-1})	C_{BC}^{max} (ng g^{-1})	f_{nonBC}^{est} (%)	$\mathring{A}_{aot}$ 450:600 nm
90	1	45°02'44"	116°22'45"	3	0	5	-14	0.38	0.15	862	530	334 (–, 473)	61 (45, 110)	3.8
91	1	50°02'48"	124°22'41"	8	0	5	-25	0.23	0.08	250	200	161 (110, 200)	35 (18, 55)	2.1
	2				5	10	-25	0.18	0.15	–	–	–	–	–
92	1	50°39'07"	122°23'53"	14	0	5	-16	0.17	0.08	80	72	53 (32, 68)	34 (15, 60)	2.3
	2				5	10	-16	0.18	1.25	108	97	77 (49, 97)	29 (11, 55)	2.2
93	1	50°24'50"	124°54'20"	8	0	1	–	–	0.07	172	97	70 (39, 90)	53 (39, 73)	2.5
	2				2	6	-21	0.21	0.175	313	136	100 (46, 128)	68 (59, 85)	2.7
94	1	50°09'05"	125°46'06"	8	0	1	-24	–	0.1	1173	404	260 (108, 363)	78 (69, 91)	2.8
95	1	50°54'43"	127°04'50"	18	0	3	-22	0.23	0.175	278	110	75 (37, 100)	73 (64, 86)	2.6
	2				3	8	-23	0.18	0.9	230	83	54 (25, 73)	77 (68, 89)	2.7
	3				8	13	-25	0.27	1	91	50	27 (7, 40)	71 (55, 92)	3.2
	4				13	18	-25	0.14	1.3	521	308	131 (–, 237)	75 (54, 148)	4.8
96	1	49°14'21"	129°43'13"	13	0	5	-22	0.37	0.08	1340	385	241 (21, 332)	83 (76, 99)	3.4
	2				5	10	-23	0.25	0.6	234	85	45 (6, 71)	81 (69, 98)	3.3
	3				10	15	-22	0.22	1	371	126	78 (26, 111)	80 (71, 93)	3.0
97	1	47°39'18"	131°13'10"	20	0	5	-22	0.36	0.2	1005	362	236 (93, 306)	76 (69, 91)	2.8
	2				5	10	-18	0.27	1.1	160	79	45 (15, 65)	71 (57, 91)	3.0
	3				10	15	-14	0.32	0.9	32	23	9 (3, 18)	74 (44, 90)	3.1
98	1	45°25'38"	130°58'55"	35	0	5	-20	0.22	0.09	2154	2080	1461 (754, 1818)	32 (16, 65)	2.5
	2				5	10	-23	0.24	0.5	641	349	241 (123, 307)	58 (46, 79)	2.6

Atmospheric
Chemistry
and Physics
Discussions

Site	Layer	Latitude N	Longitude E	Site average snow depth (cm)	Sample depth (cm) Top	Bottom	Temperature (°C)	Snow density (g cm⁻³)	Snow grain radius (mm)	C_{BC}^{equiv} (ng g⁻¹)	C_{BC}^{max} (ng g⁻¹)	C_{BC}^{max} (ng g⁻¹)	f_{nonBC}^{est} (%)	$\mathring{A}_{sot}$ 450:600 nm
	3				10	15	-15	0.24	0.75	97	55	25 (10, 45)	74 (52, 90)	3.1
	4				15	20	-14	0.26	0.75	61	39	16 (7, 31)	75 (48, 89)	3.1
	5				20	25	-13	0.28	1.1	432	261	166 (62, 221)	62 (49, 86)	2.8
	6				25	30	-11	0.29	1.3	348	165	112 (66, 148)	68 (58, 81)	2.5
	7				30	35	–	0.33	1.3	288	118	72 (37, 101)	75 (65, 87)	2.6
99	1	43°36'10"	125°42'04"	13	0	5	-2	0.18	0.085	1459	922	636 (235, 823)	54 (40, 84)	2.8
	2				5	12	-3	0.23	1.1	5847	3778	2882 (1549, 3559)	51 (39, 74)	2.5
	3				12	18	-4	0.28	1.1	2795	1360	1059 (630, 1306)	62 (53, 77)	2.3
	4				18	24	-4	0.28	0.7	2027	1518	1105 (537, 1381)	46 (32, 73)	2.6
100	1	43°30'45"	127°15'34"	18	0	2.5	–	0.14	0.075	1739	703	508 (250, 651)	71 (63, 86)	2.6
	2				2.5	4	-2	0.18	0.25	4126	2891	1729 (–, 2371)	58 (43, 103)	3.6
	3				4	9	-2	0.23	0.9	1062	564	414 (208, 529)	60 (49, 80)	2.6
	4				9	15	-3	0.24	0.8	1601	728	541 (266, 691)	66 (57, 83)	2.6
101	1	43°47'25"	125°46'08"	22	0	5	-19	0.24	0.07	5634	5070	3651 (1333, 4644)	35 (18, 76)	2.9
	2				5	10	-17	0.24	0.9	4318	3826	2575 (882, 3284)	40 (24, 79)	2.9
	3				10	15	-15	0.23	1.1	657	389	313 (206, 386)	46 (33, 63)	2.1
	4				15	20	-14	0.28	1.3	297	254	188 (108, 239)	39 (21, 67)	2.5
102	1	42°12'34"	126°37'50"	46	0	3	-8	0.13	0.07	2109	1734	1357 (808, 1755)	37 (19, 61)	2.3
	2				3	8	-8	0.26	0.1	594	377	279 (149, 371)	53 (37, 75)	2.6
	3				8	13	-8	0.24	0.3	2513	2088	1623 (425, 2120)	35 (15, 81)	3.1
	4				13	18	-8	0.28	0.6	1922	1073	773 (229, 1013)	60 (48, 88)	3.0
	5				18	23	-7	0.32	1	1112	629	450 (197, 590)	60 (47, 82)	2.7

Atmospheric Chemistry and Physics Discussions — Open Access — EGU

Site	Layer	Latitude N	Longitude E	Site average snow depth (cm)	Sample depth (cm) Top	Sample depth (cm) Bottom	Temperature (°C)	Snow density (g cm^{-3})	Snow grain radius (mm)	C_{BC}^{equiv} (ng g^{-1})	C_{BC}^{max} (ng g^{-1})	C_{BC}^{max} (ng g^{-1})	f_{nonBC}^{est} (%)	$\overset{o}{A}_{aa}$ 450:600 nm
	6				23	28	-6	0.27	1.2	1466	1281	903 (300, 1167)	38 (21, 80)	2.9
	7				28	33	-5	0.26	1.2	858	493	344 (133, 457)	66 (53, 87)	2.9
	8				33	38	-5	0.3	1	426	197	109 (27, 163)	74 (61, 95)	3.2
	9				38	43	-4	0.29	0.8	524	245	157 (67, 220)	71 (58, 87)	2.8

Atmospheric
Chemistry
and Physics
Discussions

Open Access

EGU

Table 2. Estimates of integrated snowpack BC content in seasonal snow in the study sites for 2010 and 2014.

Site	Date sampled (2014)	Snowpack average BC (ng g^{-1})	Site	Date sampled (2010)	Snowpack average BC (ng g^{-1})
90	10-Jan	334	1	11-Jan	–
91	13-Jan	161	2	12-Jan	–
92	14-Jan	65	3	12-Jan	343
93	15-Jan	94	4	13-Jan	864
94	15-Jan	260	5	13-Jan	801
95	16-Jan	62	6	13-Jan	655
96	17-Jan	140	7	15-Jan	290
97	18-Jan	105	8	15-Jan	82
98	19-Jan	264	9	16-Jan	113
99	23-Jan	1507	10	16-Jan	98
100	24-Jan	592	11	18-Jan	159
101	26-Jan	1635	12	19-Jan	641
102	27-Jan	583	13	19-Jan	413
			14	20-Jan	1781
			15	20-Jan	213
			16	21-Jan	939
			17	22-Jan	379
			18	22-Jan	424
			19	23-Jan	368
			20	24-Jan	168
			21	25-Jan	89
			22	26-Jan	55
			23	26-Jan	64
			24	26-Jan	148
			25	27-Jan	255
			26	27-Jan	193
			27	28-Jan	179
			28	29-Jan	441
			29	29-Jan	1057
			30	31-Jan	975
			31	31-Jan	749
			32	1-Feb	620
			33	2-Feb	367
			34	3-Feb	1519
			35	4-Feb	1008
			36	5-Feb	997
			37	6-Feb	815
			38	6-Feb	1596
			39	7-Feb	632
			40	8-Feb	1231

Atmospheric
Chemistry
and Physics
Discussions

Open Access

EGU

Site	Date sampled (2014)	Snowpack average BC (ng g^{-1})	Site	Date sampled (2010)	Snowpack average BC (ng g^{-1})
			41	18-Feb	–
			42	18-Feb	–
			43	19-Feb	–
			44	19-Feb	–
			45	19-Feb	–
			46	20-Feb	–

Atmospheric
Chemistry
and Physics
Discussions

Table 3. Chemical species (ng g^{-1}) in surface snow for sites across northeastern China in January 2014.

Site	AD	BC	OC	K$^+_{biosmoke}$	SO$_4^{2-}$	NO$_3^-$	NH$_4^+$	Sea salt
90	1900	380	6700	327	1685	213	22	868
91	1700	180	590	179	853	465	36	827
92	1300	60	280	150	511	105	19	456
93	1700	80	450	213	718	387	90	960
94	3300	300	2700	118	1335	550	28	554
95	2000	90	600	164	587	523	39	669
96	2300	280	3900	309	1285	493	91	1227
97	2400	280	2400	173	1163	407	38	753
98	3900	1600	13300	633	3096	747	195	2516
99	3000	770	4700	372	3379	1492	155	2310
100	3800	570	4000	260	4237	2258	487	2195
101	3500	4200	32000	1337	12382	2364	–	5131
102	5800	1700	2400	488	8034	3631	769	4420

Table 4. Measured and calculated snow grain sizes for sites in northeastern China in January 2014.

| Site	Measured Snow grain radius (μm)	Calculated R$_{eff}$ using SAMDS (μm)	Calculated R$_{eff}$ using SNICAR (μm)
90	150	203-236	168-197
91	80	178-220	148-183
93	70	73-80	60-65
95	175	148-188	123-156
98	90	248-302	209-259
101	70	362-446	312-390

Atmospheric
Chemistry
and Physics
Discussions
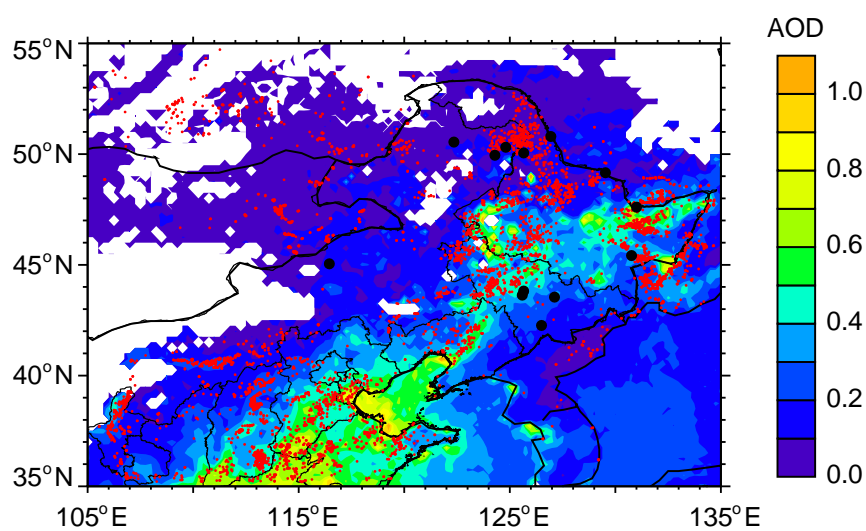
Fig. 1. Spatial distribution of the averaged AOD retrieved from Aqua-MODIS over northern China from October to January; the red regions are MODIS active fire locations; the black dots are the sampling locations.
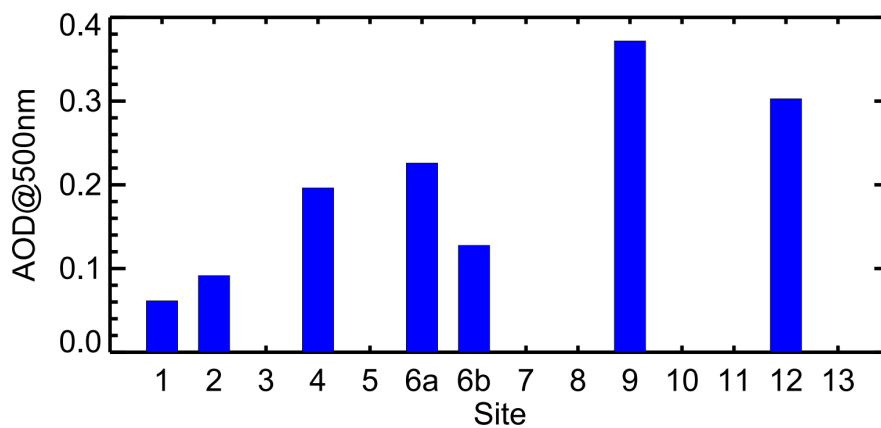
Fig. 2. The variation in AOD at different sites measured using a Microtops Π Sun photometer over northern China in January 2014.

Atmospheric
Chemistry
and Physics
Discussions

Open Access
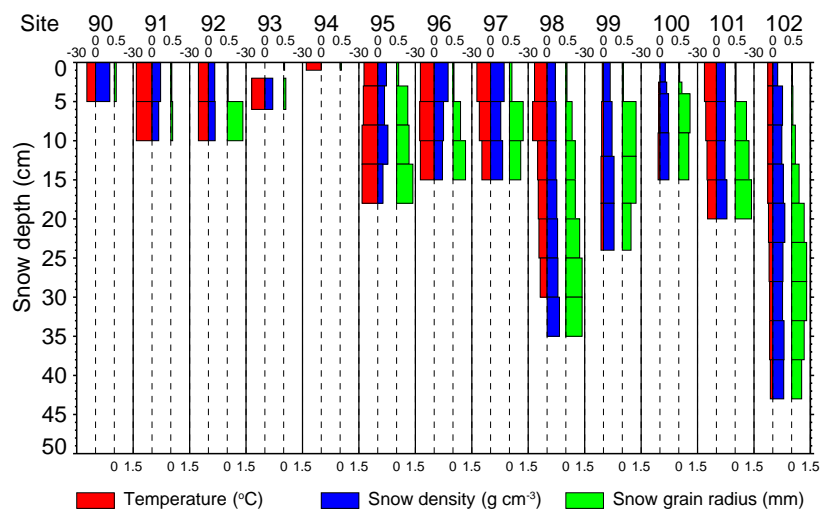
Fig. 3. Vertical temperature, snow density, and snow grain radius profiles at each site during the 2014 Chinese snow survey.
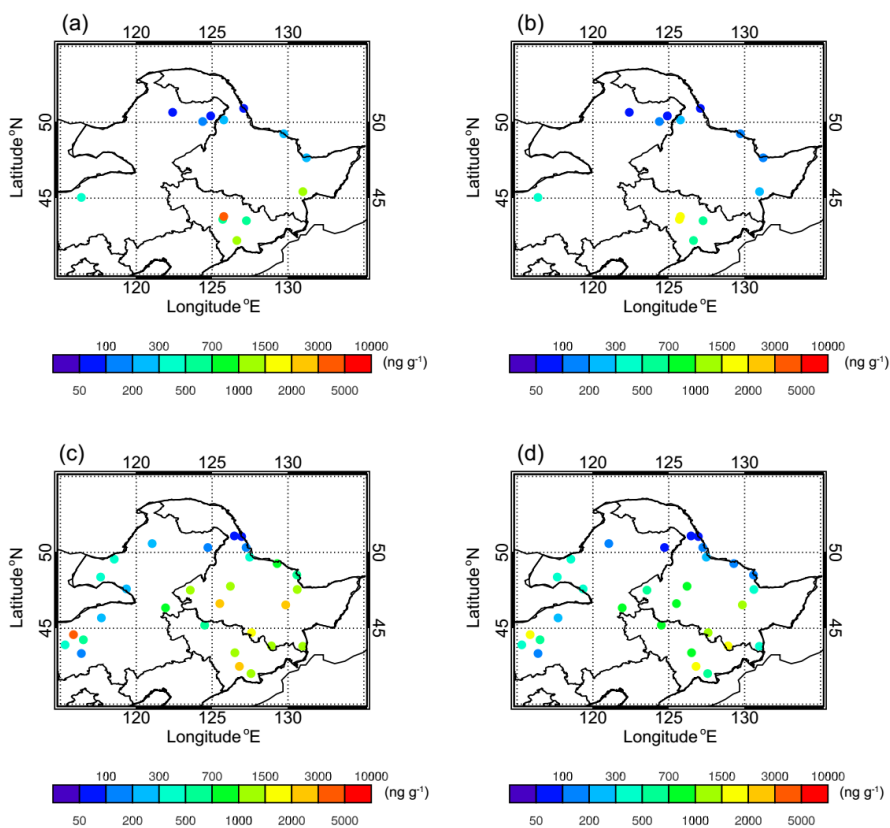
Fig. 4. Surface (a, c) and averaged and integrated (b, d) BC content in seasonal snow in 2014 and 2010 across northern China.
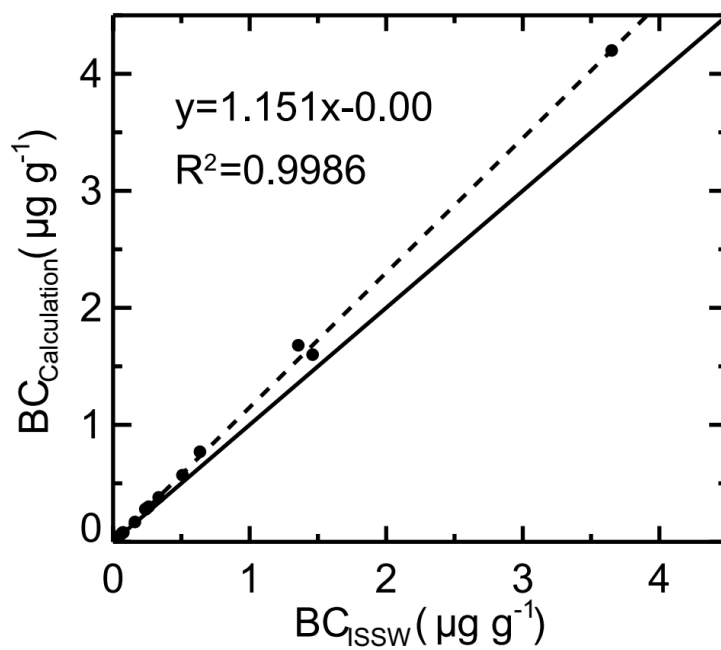
Fig. 5. Comparisons between the calculated and optically measured BC contents in surface snow in January 2014.
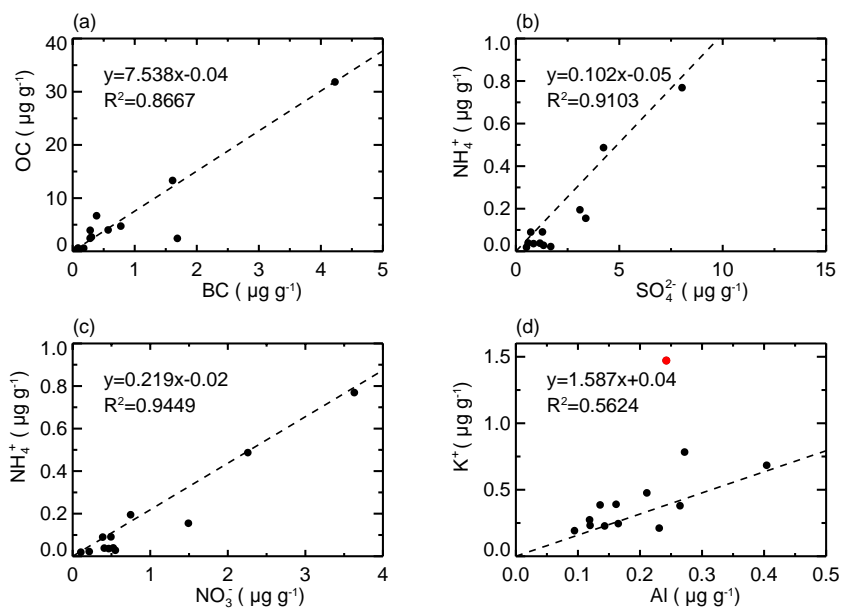
Fig. 6. Ratios of OC and BC, NH_4^+ and SO_4^{2-}, NH_4^+ and NO_3^-, and K^+ and Al in surface snow in January 2014.
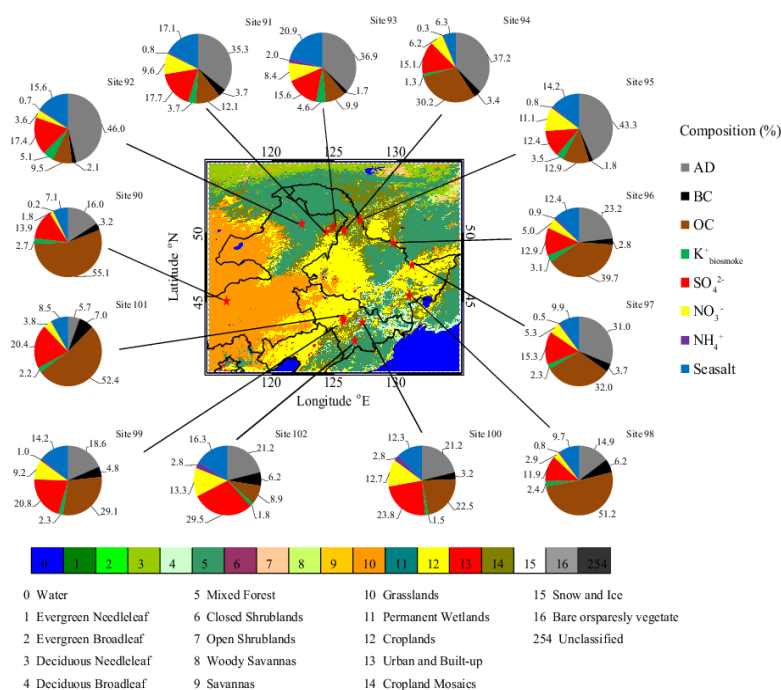
Fig. 7. The major components include AD, BC, OC, biomass smoke potassium, secondary aerosol ions (sulfate, nitrate, and ammonium), and sea salt in the surface snow samples collected in January 2014.
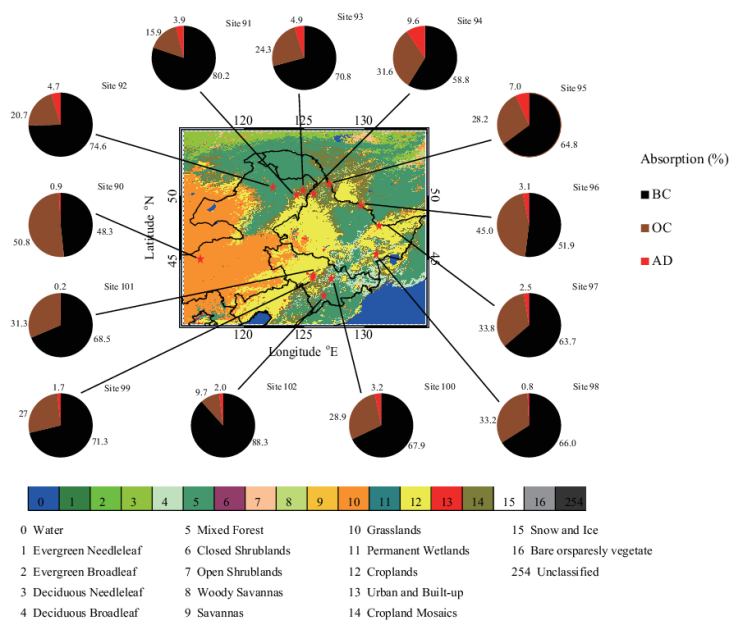
Fig. 8. The light absorption of ILAPs in surface snow in January 2014.
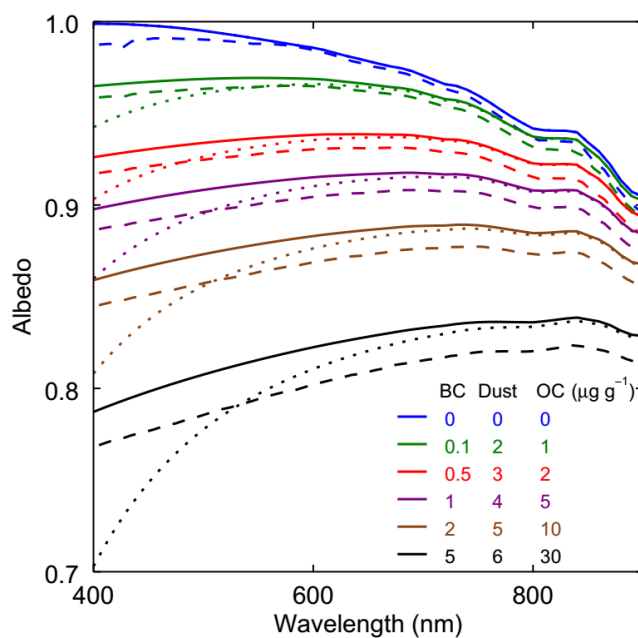
Fig. 9. Spectral albedo of snow with different contaminants for a 60° solar zenith angle and a 70 µm snow grain radius. (Solid and dashed lines show the SAMDS and SNICAR model predictions of BC and mineral dust. Dotted lines show the SAMDS model predictions for all ILAPs, including BC, mineral dust, and OC).
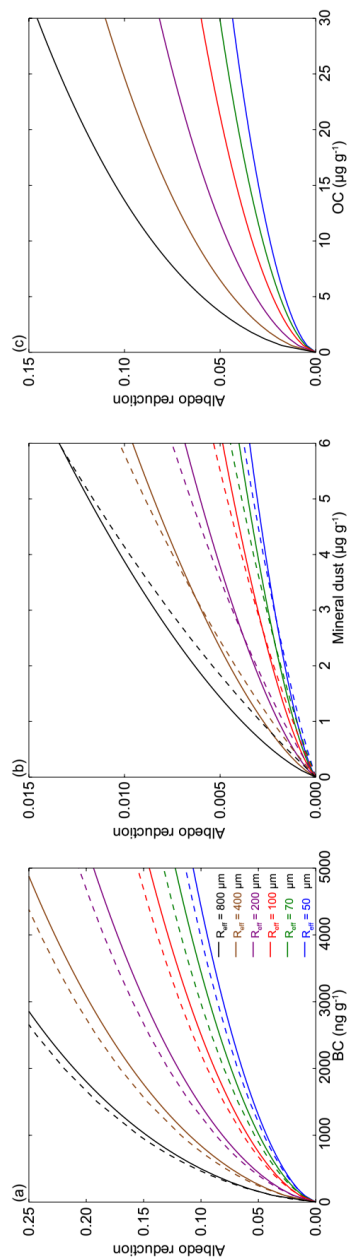
Fig. 10. Spectrally weighted snow albedo reduction over the 400–1400 nm solar spectrum attributed to (a) BC, (b) mineral dust, and (c) OC computed as the albedo of pure snow minus the albedo of contaminated snow for a 60° solar zenith angle. (Solid and dashed lines show the SAMDS and SNICAR models predictions. The MAC values of BC, Fe, and OC were assumed to be 7.5 m^2 g^{-1}, 0.9 m^2 g^{-1}, and 0.3 m^2 g^{-1} at 550 nm, respectively).
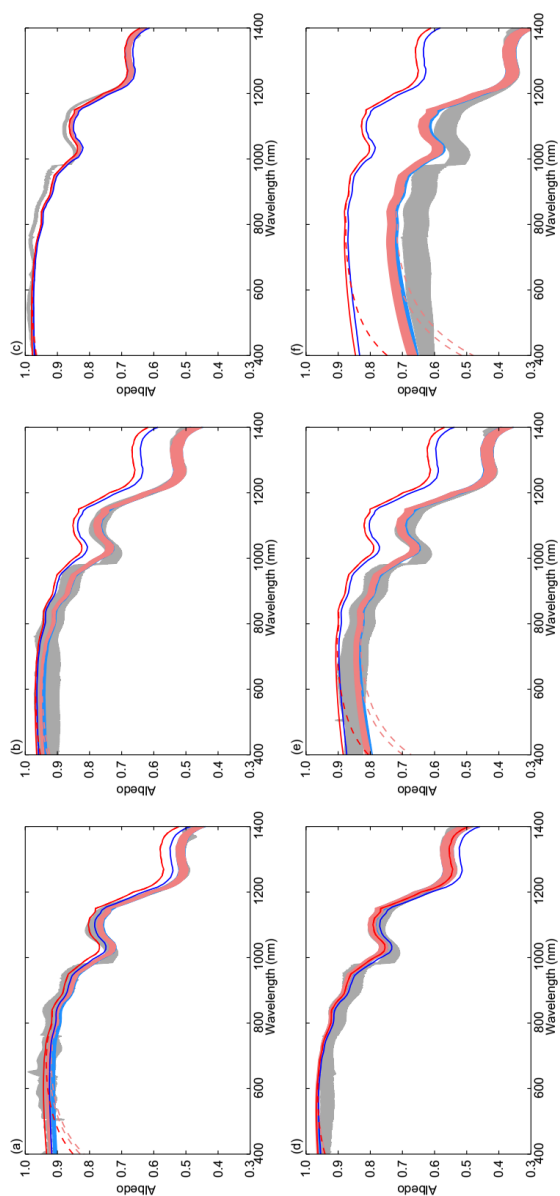
Fig. 11. Measured and modeled spectral albedos of snow at sites (a) 90, (b) 91, (c) 93, (d) 95, (e) 98, and (f) 101. (Gray shaded bands correspond to measured spectral albedos, red and blue solid lines correspond to spectral albedos from the SAMDS and SNICAR models with measured snow grain radii, and red and blue shaded bands correspond to the albedos from the SAMDS and SNICAR models with calculated snow grain optical effective radii (R_{eff}). Contaminants only include BC and mineral dust in the SAMDS and SNICAR models. In the SNICAR model, the ratio of Fe in dust was found to be 2.8%. Dashed red lines are similar to solid red lines, although OC should be added to the list of contaminants in the model.

Atmospheric
Chemistry
and Physics
Discussions

References

Acosta, J. A., Faz, A., Kalbitz, K., Jansen, B., and Martinez-Martinez, S.: Heavy metal concentrations in particle size fractions from street dust of Murcia (Spain) as the basis for risk assessment, J. Environ. Monitor., 13, 3087-3096, 10.1039/c1em10364d, 2011.

Aleksandropoulou, V., Torseth, K., and Lazaridis, M.: Atmospheric Emission Inventory for Natural and Anthropogenic Sources and Spatial Emission Mapping for the Greater Athens Area, Water Air Soil Pollut., 219, 507-526, 10.1007/s11270-010-0724-2, 2011.

Arhami, M., Kuhn, T., Fine, P. M., Delfino, R. J., and Sioutas, C.: Effects of sampling artifacts and operating parameters on the performance of a semicontinuous particulate elemental carbon/organic carbon monitor, Environ. Sci. Technol., 40, 945-954, 10.1021/es0510313, 2006.

Ax, W., Malchow, H., Koren, H., and Fischer, H.: Studies on immunological reactions in vitro, Sbornik vedeckych praci Lekarske fakulty Karlovy university v Hradci Kralove, 13, 287-292, 1970.

Bergstrom, R. W., Russell, P. B., and Hignett, P.: Wavelength dependence of the absorption of black carbon particles: Predictions and results from the TARFOX experiment and implications for the aerosol single scattering albedo, J. Atmos. Sci., 59, 567-577, Doi 10.1175/1520-0469(2002)059<0567:Wdotao>2.0.Co;2, 2002.

Bi, J. R., Huang, J. P., Hu, Z. Y., Holben, B. N., and Guo, Z. Q.: Investigating the aerosol optical and radiative characteristics of heavy haze episodes in Beijing during January of 2013, J. Geophys. Res.-Atmos., 119, 9884-9900, 10.1002/2014JD021757, 2014.

Bond, T. C., Bussemer, M., Wehner, B., Keller, S., Charlson, R. J., and Heintzenberg, J.: Light absorption by primary particle emissions from a lignite burning plant, Environ. Sci. Technol., 33, 3887-3891, Doi 10.1021/Es9810538, 1999.

Bond, T. C., and Bergstrom, R. W.: Light absorption by carbonaceous particles: An investigative review, Aerosol Sci. Tech., 40, 27-67, 10.1080/02786820500421521, 2006.

Bond, T. C., Doherty, S. J., Fahey, D. W., Forster, P. M., Berntsen, T., DeAngelo, B. J., Flanner, M. G., Ghan, S., Karcher, B., Koch, D., Kinne, S., Kondo, Y., Quinn, P. K., Sarofim, M. C., Schultz, M. G., Schulz, M., Venkataraman, C., Zhang, H., Zhang, S., Bellouin, N., Guttikunda, S. K., Hopke, P. K., Jacobson, M. Z., Kaiser, J. W., Klimont, Z., Lohmann, U., Schwarz, J. P., Shindell, D., Storelvmo, T., Warren, S. G., and Zender, C. S.: Bounding the role of black carbon in the climate system: A scientific assessment, J. Geophys. Res.-Atmos., 118, 5380-5552, 10.1002/jgrd.50171, 2013.

Brandt, R. E., Warren, S. G., and Clarke, A. D.: A controlled snowmaking experiment testing the relation between black carbon content and reduction of snow albedo, J. Geophys. Res.-Atmos., 116, Artn D08109, 10.1029/2010jd015330, 2011.

Cachier, H., Liousse, C., Buatmenard, P., and Gaudichet, A.: Particulate Content of Savanna Fire Emissions, J. Atmos. Chem., 22, 123-148, Doi 10.1007/Bf00708185, 1995.

Cao, J. J., Lee, S. C., Chow, J. C., Watson, J. G., Ho, K. F., Zhang, R. J., Jin, Z. D., Shen, Z. X., Chen, G. C., Kang, Y. M., Zou, S. C., Zhang, L. Z., Qi, S. H., Dai, M. H., Cheng, Y., and Hu, K.: Spatial and seasonal distributions of carbonaceous aerosols over China, J. Geophys. Res.-Atmos., 112, Artn D22s11, 10.1029/2006jd008205, 2007.

Carmagnola, C. M., Domine, F., Dumont, M., Wright, P., Strellis, B., Bergin, M., Dibb, J., Picard, G., Libois, Q., Arnaud, L., and Morin, S.: Snow spectral albedo at Summit, Greenland: measurements and numerical simulations based on physical and chemical properties of the snowpack, Cryosphere, 7, 1139-1160, 10.5194/tc-7-1139-2013, 2013.

Che, H., Zhang, X. Y., Xia, X., Goloub, P., Holben, B., Zhao, H., Wang, Y., Zhang, X. C., Wang, H., Blarel, L., Damiri, B., Zhang, R., Deng, X., Ma, Y., Wang, T., Geng, F., Qi, B., Zhu, J., Yu, J., Chen, Q., and Shi, G.: Ground-based aerosol climatology of China: aerosol optical depths from the China Aerosol Remote Sensing Network (CARSNET) 2002-2013, Atmos. Chem. Phys., 15, 7619-7652, 10.5194/acp-15-7619-2015, 2015a.

Che, H. Z., Yang, Z. F., Zhang, X. Y., Zhu, C. Z., Ma, Q. L., Zhou, H. G., and Wang, P.: Study on the aerosol optical properties and their relationship with aerosol chemical compositions over three regional background stations in China, Atmos. Environ., 43, 1093-1099, 10.1016/j.atmosenv.2008.11.010, 2009.

Che, H. Z., Wang, Y. Q., and Sun, J. Y.: Aerosol optical properties at Mt. Waliguan Observatory, China, Atmos. Environ., 45, 6004-6009, 10.1016/j.atmosenv.2011.07.050, 2011.

Che, H. Z., Wang, Y. Q., Sun, J. Y., Zhang, X. C., Zhang, X. Y., and Guo, J. P.: Variation of Aerosol Optical Properties over the Taklimakan Desert in China, Aerosol Air Qual. Res., 13, 777-785, 10.4209/aaqr.2012.07.0200, 2013.

Che, H. Z., Zhao, H. J., Wu, Y. F., Xia, X. G., Zhu, J., Wang, H., Wang, Y. Q., Sun, J. Y., Yu, J., Zhang, X. Y., and Shi, G. Y.: Analyses of aerosol optical properties and direct radiative forcing over urban and industrial regions in Northeast China, Meteorol. Atmos. Phys., 127, 345-354, 10.1007/s00703-015-0367-3, 2015b.

Chen, S. Y., Huang, J. P., Zhao, C., Qian, Y., Leung, L. R., and Yang, B.: Modeling the transport and radiative forcing of Taklimakan dust over the Tibetan Plateau: A case study in the summer of 2006, J. Geophys. Res.-Atmos., 118, 797-812, 10.1002/jgrd.50122, 2013.

Chu, D. A., Kaufman, Y. J., Ichoku, C., Remer, L. A., Tanre, D., and Holben, B. N.: Validation of MODIS aerosol optical depth retrieval over land, Geophys. Res. Lett., 29, Artn 1617, 10.1029/2001gl013205, 2002.

Cong, Z., Kang, S., Kawamura, K., Liu, B., Wan, X., Wang, Z., Gao, S., and Fu, P.: Carbonaceous aerosols on the south edge of the Tibetan Plateau: concentrations, seasonality and sources, Atmos. Chem. Phys., 15, 1573-1584, 10.5194/acp-15-1573-2015, 2015.

Coz, E., Casuccio, G., Lersch, T. L., Moreno, T., and Artinano, B.: Anthropogenic Influenced Mineral Dust Ambient Fine Particles At An Urban Site In Barcelona (Spain), Chem. Eng. Trans., 22, 101-106, 10.3303/Cet1022016, 2010.

Dang, C., and Hegg, D. A.: Quantifying light absorption by organic carbon in Western North American snow by serial chemical extractions, J. Geophys. Res.-Atmos., 119, 10.1002/2014JD022156, 2014.

de Mourgues, G., Fischer, L., and Felman, D.: Salter's" innominate osteotomy" of the pelvis for inequality of inferior limbs in a child, after complex injuries of the pelvis and one femur, Lyon chirurgical, 66, 62, 1970.

Doherty, S. J., Warren, S. G., Grenfell, T. C., Clarke, A. D., and Brandt, R. E.: Light-absorbing impurities in Arctic snow, Atmos. Chem. Phys., 10, 11647-11680, 10.5194/acp-10-11647-2010, 2010.

Doherty, S. J., Grenfell, T. C., Forsstrom, S., Hegg, D. L., Brandt, R. E., and Warren, S. G.: Observed vertical redistribution of black carbon and other insoluble light-

absorbing particles in melting snow, J. Geophys. Res.-Atmos., 118, 5553-5569, 10.1002/jgrd.50235, 2013.

Doherty, S. J., Dang, C., Hegg, D. A., Zhang, R. D., and Warren, S. G.: Black carbon and other light-absorbing particles in snow of central North America, J. Geophys. Res.-Atmos., 119, 12807-12831, 10.1002/2014JD022350, 2014.

Flanner, M. G., Zender, C. S., Randerson, J. T., and Rasch, P. J.: Present-day climate forcing and response from black carbon in snow, J. Geophys. Res.-Atmos., 112, Artn D11202, 10.1029/2006jd008003, 2007.

Flanner, M. G., Zender, C. S., Hess, P. G., Mahowald, N. M., Painter, T. H., Ramanathan, V., and Rasch, P. J.: Springtime warming and reduced snow cover from carbonaceous particles, Atmos. Chem. Phys., 9, 2481-2497, 2009.

Flanner, M. G.: Arctic climate sensitivity to local black carbon, J. Geophys. Res.-Atmos., 118, 1840-1851, 10.1002/jgrd.50176, 2013.

Friedl, M. A., Sulla-Menashe, D., Tan, B., Schneider, A., Ramankutty, N., Sibley, A., and Huang, X. M.: MODIS Collection 5 global land cover: Algorithm refinements and characterization of new datasets, Remote Sens. Environ., 114, 168-182, 10.1016/j.rse.2009.08.016, 2010.

Ginoux, P., Garbuzov, D., and Hsu, N. C.: Identification of anthropogenic and natural dust sources using Moderate Resolution Imaging Spectroradiometer (MODIS) Deep Blue level 2 data, J. Geophys. Res.-Atmos., 115, Artn D05204, 10.1029/2009jd012398, 2010.

Givati, A., and Rosenfeld, D.: Quantifying precipitation suppression due to air pollution, J. Appl. Meteorol., 43, 1038-1056, Doi 10.1175/1520-0450(2004)043<1038:Qpsdta>2.0.Co;2, 2004.

Goudie, A. S., and Middleton, N. J.: Saharan dust storms: nature and consequences, Earth Sci. Rev., 56, 179-204, Doi 10.1016/S0012-8252(01)00067-8, 2001.

Grenfell, T. C., Doherty, S. J., Clarke, A. D., and Warren, S. G.: Light absorption from particulate impurities in snow and ice determined by spectrophotometric analysis of filters, Appl. Opt., 50, 2037-2048, 10.1364/Ao.50.002037, 2011.

Guan, X., Huang, J., Guo, R., Yu, H., Lin, P., and Zhang, Y.: Role of radiatively forced temperature changes in enhanced semi-arid warming in the cold season over east Asia, Atmos. Chem. Phys., 15, 13777-13786, 10.5194/acp-15-13777-2015, 2015.

Hadley, O. L., and Kirchstetter, T. W.: Black-carbon reduction of snow albedo, Nat. Clim. Change, 2, 437-440, 10.1038/Nclimate1433, 2012.

Hansen, J., and Nazarenko, L.: Soot climate forcing via snow and ice albedos, PNAS 101, 423-428, 10.1073/pnas.2237157100, 2004.

Hansen, J., Sato, M., Ruedy, R., Nazarenko, L., Lacis, A., Schmidt, G. A., Russell, G., Aleinov, I., Bauer, M., Bauer, S., Bell, N., Cairns, B., Canuto, V., Chandler, M., Cheng, Y., Del Genio, A., Faluvegi, G., Fleming, E., Friend, A., Hall, T., Jackman, C., Kelley, M., Kiang, N., Koch, D., Lean, J., Lerner, J., Lo, K., Menon, S., Miller, R., Minnis, P., Novakov, T., Oinas, V., Perlwitz, J., Perlwitz, J., Rind, D., Romanou, A., Shindell, D., Stone, P., Sun, S., Tausnev, N., Thresher, D., Wielicki, B., Wong, T., Yao, M., and Zhang, S.: Efficacy of climate forcings, J. Geophys. Res.-Atmos., 110, Artn D18104, 10.1029/2005jd005776, 2005.

Hegg, D. A., Warren, S. G., Grenfell, T. C., Doherty, S. J., Larson, T. V., and Clarke, A. D.: Source Attribution of Black Carbon in Arctic Snow, Environ. Sci. Technol., 43, 4016-4021, 10.1021/es803623f, 2009.

Hegg, D. A., Warren, S. G., Grenfell, T. C., Doherty, S. J., and Clarke, A. D.: Sources of light-absorbing aerosol in arctic snow and their seasonal variation, Atmos. Chem. Phys., 10, 10923-10938, 10.5194/acp-10-10923-2010, 2010.

Atmospheric
Chemistry
and Physics
Discussions

Open Access

Holben, B. N., Eck, T. F., and Fraser, R. S.: Temporal and Spatial Variability of Aerosol Optical Depth in the Sahel Region in Relation to Vegetation Remote-Sensing, Int. J. Remote Sens., 12, 1147-1163, 1991.

Holben, B. N., Tanre, D., Smirnov, A., Eck, T. F., Slutsker, I., Abuhassan, N., Newcomb, W. W., Schafer, J. S., Chatenet, B., Lavenu, F., Kaufman, Y. J., Castle, J. V., Setzer, A., Markham, B., Clark, D., Frouin, R., Halthore, R., Karneli, A., O'Neill, N. T., Pietras, C., Pinker, R. T., Voss, K., and Zibordi, G.: An emerging ground-based aerosol climatology: Aerosol optical depth from AERONET, J. Geophys. Res.-Atmos., 106, 12067-12097, Doi 10.1029/2001jd900014, 2001.

Holben, B. N., Eck, T. F., Slutsker, I., Smirnov, A., Sinyuk, A., Schafer, J., Giles, D., and Dubovik, O.: AERONET's Version 2.0 quality assurance criteria - art. no. 64080Q, Remote Sensing of the Atmosphere and Clouds, 6408, Q4080-Q4080, Artn 64080q, 10.1117/12.706524, 2006.

Hsu, S. C., Liu, S. C., Huang, Y. T., Chou, C. C. K., Lung, S. C. C., Liu, T. H., Tu, J. Y., and Tsai, F. J.: Long-range southeastward transport of Asian biosmoke pollution: Signature detected by aerosol potassium in Northern Taiwan, J. Geophys. Res.-Atmos., 114, Artn D14301, 10.1029/2009jd011725, 2009.

Huang, J. P., Fu, Q. A., Zhang, W., Wang, X., Zhang, R. D., Ye, H., and Warren, S. G.: Dust and Black Carbon in Seasonal Snow across Northern China, Bull. Amer. Meteor. Soc., 92, 175-181, 10.1175/2010BAMS3064.1, 2011.

Huang, J. P., Wang, T. H., Wang, W. C., Li, Z. Q., and Yan, H. R.: Climate effects of dust aerosols over East Asian arid and semiarid regions, J. Geophys. Res.-Atmos., 119, 11398-11416, 10.1002/2014JD021796, 2014.

Huang, J. P., Liu, J. J., Chen, B., and Nasiri, S. L.: Detection of anthropogenic dust using CALIPSO lidar measurements, Atmos. Chem. Phys., 15, 11653-11665, 10.5194/acp-15-11653-2015, 2015a.

Huang, Z. W., Huang, J. P., Hayasaka, T., Wang, S. S., Zhou, T., and Jin, H. C.: Short-cut transport path for Asian dust directly to the Arctic: a case study, Environ. Res. Lett., 10, Artn 114018, 10.1088/1748-9326/10/11/114018, 2015b.

Ianniello, A., Spataro, F., Esposito, G., Allegrini, I., Hu, M., and Zhu, T.: Chemical characteristics of inorganic ammonium salts in PM2.5 in the atmosphere of Beijing (China), Atmos. Chem. Phys., 11, 10803-10822, 10.5194/acp-11-10803-2011, 2011.

Ichoku, C., Chu, D. A., Mattoo, S., Kaufman, Y. J., Remer, L. A., Tanre, D., Slutsker, I., and Holben, B. N.: A spatio-temporal approach for global validation and analysis of MODIS aerosol products, Geophys. Res. Lett., 29, Artn 1616, 10.1029/2001gl013206, 2002a.

Ichoku, C., Levy, R., Kaufman, Y. J., Remer, L. A., Li, R. R., Martins, V. J., Holben, B. N., Abuhassan, N., Slutsker, I., Eck, T. F., and Pietras, C.: Analysis of the performance characteristics of the five-channel Microtops II Sun photometer for measuring aerosol optical thickness and precipitable water vapor, J. Geophys. Res.-Atmos., 107, Artn 4179, 10.1029/2001jd001302, 2002b.

IPCC: Climate Change 2013: The Physical Science Basis. Contribution of Working Group I to the Fifth Assessment Report of the Intergovernmental Panel on Climate Change, Stocker, T. F., Qin, D., Plattner, G.-K., Tignor, M., Allen, S. K., Boschung, J., Nauels, A., Xia, Y., Bex, V., and Midgley, P. M., Cambridge Univ. Press, Cambridge, United Kingdom and New York, NY, USA, 2013.

Jacobson, M. Z.: Climate response of fossil fuel and biofuel soot, accounting for soot's feedback to snow and sea ice albedo and emissivity, J. Geophys. Res.-Atmos., 109, Artn D21201, 10.1029/2004jd004945, 2004.

Atmospheric
Chemistry
and Physics
Discussions

Kamani, H., Ashrafi, S. D., Isazadeh, S., Jaafari, J., Hoseini, M., Mostafapour, F. K., Bazrafshan, E., Nazmara, S., and Mahvi, A. H.: Heavy Metal Contamination in Street Dusts with Various Land Uses in Zahedan, Iran, B. Environ. Contam. Tox., 94, 382-386, 10.1007/s00128-014-1453-9, 2015.

Kang, L. T., Huang, J. P., Chen, S. Y., and Wang, X.: Long-term trends of dust events over Tibetan Plateau during 1961-2010, Atmos. Environ., 125, 188-198, 10.1016/j.atmosenv.2015.10.085, 2016.

Kaufman, Y. J., Tanre, D., Gordon, H. R., Nakajima, T., Lenoble, J., Frouin, R., Grassl, H., Herman, B. M., King, M. D., and Teillet, P. M.: Passive remote sensing of tropospheric aerosol and atmospheric correction for the aerosol effect, J. Geophys. Res.-Atmos., 102, 16815-16830, Doi 10.1029/97jd01496, 1997.

Kim, W., Doh, S. J., and Yu, Y.: Anthropogenic contribution of magnetic particulates in urban roadside dust, Atmos. Environ., 43, 3137-3144, 10.1016/j.atmosenv.2009.02.056, 2009.

Koch, D., Menon, S., Del Genio, A., Ruedy, R., Alienov, I., and Schmidt, G. A.: Distinguishing Aerosol Impacts on Climate over the Past Century, J. Climate, 22, 2659-2677, 10.1175/2008JCLI2573.1, 2009.

Kokhanovsky, A. A., and Zege, E. P.: Scattering optics of snow, Appl. Opt., 43, 1589-1602, Doi 10.1364/Ao.43.001589, 2004.

Kotthaus, S., Smith, T. E. L., Wooster, M. J., and Grimmond, C. S. B.: Derivation of an urban materials spectral library through emittance and reflectance spectroscopy, Isprs J. Photogramm., 94, 194-212, 10.1016/j.isprsjprs.2014.05.005, 2014.

Lafon, S., Sokolik, I. N., Rajot, J. L., Caquineau, S., and Gaudichet, A.: Characterization of iron oxides in mineral dust aerosols: Implications for light absorption, J. Geophys. Res.-Atmos., 111, Artn D21207. 10.1029/2005jd007016, 2006.

Li, G. J., Chen, J., Ji, J. F., Yang, J. D., and Conway, T. M.: Natural and anthropogenic sources of East Asian dust, Geology, 37, 727-730, 10.1130/G30031a.1, 2009.

Li, S. Y., Lei, J. Q., Xu, X. W., Wang, H. F., and Gu, F.: Dust Source of Sandstorm in the Tarim Basin, Northwest China, Adv. Environ. Sci. Eng., 518-523, 4592-4598, 10.4028/www.scientific.net/AMR.518-523.4592, 2012.

Li, X. Y., Liu, L. J., Wang, Y. G., Luo, G. P., Chen, X., Yang, X. L., Hall, M. H. P., Guo, R. C., Wang, H. J., Cui, J. H., and He, X. Y.: Heavy metal contamination of urban soil in an old industrial city (Shenyang) in Northeast China, Geoderma, 192, 50-58, 10.1016/j.geoderma.2012.08.011, 2013.

Light, B., Eicken, H., Maykut, G. A., and Grenfell, T. C.: The effect of included particulates on the spectral albedo of sea ice, J. Geophys. Res.-Oceans, 103, 27739-27752, Doi 10.1029/98jc02587, 1998.

Lorenz, K., Preston, C. M., and Kandeler, E.: Soil organic matter in urban soils: Estimation of elemental carbon by thermal oxidation and characterization of organic matter by solid-state C-13 nuclear magnetic resonance (NMR) spectroscopy, Geoderma, 130, 312-323, 10.1016/j.geoderma.2005.02.004, 2006.

Loveland, T. R., and Belward, A. S.: The IGBP-DIS global 1 km land cover data set, DISCover: first results, Int. J. Remote Sens., 18, 3291-3295, 1997.

Mahowald, N. M., and Luo, C.: A less dusty future?, Geophys. Res. Lett., 30, Artn 1903, 10.1029/2003gl017880, 2003.

Mahowald, N. M., Baker, A. R., Bergametti, G., Brooks, N., Duce, R. A., Jickells, T. D., Kubilay, N., Prospero, J. M., and Tegen, I.: Atmospheric global dust cycle and iron inputs to the ocean, Global Biogeochem. CY., 19, Artn Gb4025, 10.1029/2004gb002402, 2005.

Atmospheric
Chemistry
and Physics
Discussions

Open Access

Ming, J., Xiao, C. D., Sun, J. Y., Kang, S. C., and Bonasoni, P.: Carbonaceous particles in the atmosphere and precipitation of the Nam Co region, central Tibet, J. Environ. Sci., 22, 1748-1756, 10.1016/S1001-0742(09)60315-6, 2010.

Morys, M., Mims, F. M., Hagerup, S., Anderson, S. E., Baker, A., Kia, J., and Walkup, T.: Design, calibration, and performance of MICROTOPS II handheld ozone monitor and Sun photometer, J. Geophys. Res.-Atmos., 106, 14573-14582, Doi 10.1029/2001jd900103, 2001.

Motoyoshi, H., Aoki, T., Hori, M., Abe, O., and Mochizuki, S.: Possible effect of anthropogenic aerosol deposition on snow albedo reduction at Shinjo, Japan, J. Meteorol. Soc. Jpn., 83A, 137-148, Doi 10.2151/Jmsj.83a.137, 2005.

Novakov, T., Menon, S., Kirchstetter, T. W., Koch, D., and Hansen, J. E.: Aerosol organic carbon to black carbon ratios: Analysis of published data and implications for climate forcing, J. Geophys. Res.-Atmos., 110, Artn D21205, 10.1029/2005jd005977, 2005.

Painter, T. H., Barrett, A. P., Landry, C. C., Neff, J. C., Cassidy, M. P., Lawrence, C. R., McBride, K. E., and Farmer, G. L.: Impact of disturbed desert soils on duration of mountain snow cover, Geophys. Res. Lett., 34, Artn L12502, 10.1029/2007gl030284, 2007.

Painter, T. H., Deems, J. S., Belnap, J., Hamlet, A. F., Landry, C. C., and Udall, B.: Response of Colorado River runoff to dust radiative forcing in snow, PNAS 107, 17125-17130, 10.1073/pnas.0913139107, 2010.

Painter, T. H., Bryant, A. C., and Skiles, S. M.: Radiative forcing by light absorbing impurities in snow from MODIS surface reflectance data, Geophys. Res. Lett., 39, Artn L17502, 10.1029/2012gl052457, 2012.

Painter, T. H., Seidel, F. C., Bryant, A. C., Skiles, S. M., and Rittger, K.: Imaging spectroscopy of albedo and radiative forcing by light-absorbing impurities in mountain snow, J. Geophys. Res.-Atmos., 118, 9511-9523, 10.1002/jgrd.50520, 2013.

Park, S. U., and Park, M. S.: Aerosol size distributions observed at Naiman in the Asian dust source region of Inner Mongolia, Atmos. Environ., 82, 17-23, 10.1016/j.atmosenv.2013.09.054, 2014.

Pedersen, C. A., Gallet, J. C., Strom, J., Gerland, S., Hudson, S. R., Forsstrom, S., Isaksson, E., and Berntsen, T. K.: In situ observations of black carbon in snow and the corresponding spectral surface albedo reduction, J. Geophys. Res.-Atmos., 120, 1476-1489, 10.1002/2014JD022407, 2015.

Pio, C. A., Legrand, M., Oliveira, T., Afonso, J., Santos, C., Caseiro, A., Fialho, P., Barata, F., Puxbaum, H., Sanchez-Ochoa, A., Kasper-Giebl, A., Gelencser, A., Preunkert, S., and Schock, M.: Climatology of aerosol composition (organic versus inorganic) at nonurban sites on a west-east transect across Europe, J. Geophys. Res.-Atmos., 112, Artn D23s02, 10.1029/2006jd008038, 2007.

Porter, J. N., Miller, M., Pietras, C., and Motell, C.: Ship-based sun photometer measurements using Microtops sun photometers, J. Atmos. Oceanic Technol., 18, 765-774, Doi 10.1175/1520-0426(2001)018<0765:Sbspmu>2.0.Co;2, 2001.

Pu, W., Wang, X., Zhang, X. Y., Ren, Y., Shi, J. S., Bi, J. R., and Zhang, B. D.: Size Distribution and Optical Properties of Particulate Matter (PM10) and Black Carbon (BC) during Dust Storms and Local Air Pollution Events across a Loess Plateau Site, Aerosol Air Qual. Res., 15, 2212-2224, 10.4209/aaqr.2015.02.0109, 2015.

Qian, Y., Wang, H. L., Zhang, R. D., Flanner, M. G., and Rasch, P. J.: A sensitivity study on modeling black carbon in snow and its radiative forcing over the Arctic

and Northern China, Environ. Res. Lett., 9, Artn 064001, 10.1088/1748-9326/9/6/064001, 2014.

Qian, Y., Yasunari, T. J., Doherty, S. J., Flanner, M. G., Lau, W. K. M., Ming, J., Wang, H. L., Wang, M., Warren, S. G., and Zhang, R. D.: Light-absorbing Particles in Snow and Ice: Measurement and Modeling of Climatic and Hydrological impact, Adv. Atmos. Sci., 32, 64-91, 10.1007/s00376-014-0010-0, 2015.

Qiao, Q. Q., Huang, B. C., Zhang, C. X., Piper, J. D. A., Pan, Y. P., and Sun, Y.: Assessment of heavy metal contamination of dustfall in northern China from integrated chemical and magnetic investigation, Atmos. Environ., 74, 182-193, 10.1016/j.atmosenv.2013.03.039, 2013.

Remer, L. A., Tanre, D., Kaufman, Y. J., Ichoku, C., Mattoo, S., Levy, R., Chu, D. A., Holben, B., Dubovik, O., Smirnov, A., Martins, J. V., Li, R. R., and Ahmad, Z.: Validation of MODIS aerosol retrieval over ocean, Geophys. Res. Lett., 29, Artn 1618, 10.1029/2001gl013204, 2002.

Rosenfeld, D., Rudich, Y., and Lahav, R.: Desert dust suppressing precipitation: A possible desertification feedback loop, PNAS 98, 5975-5980, DOI 10.1073/pnas.101122798, 2001.

Routray, A., Mohanty, U. C., Osuri, K. K., and Prasad, S. K.: Improvement of Monsoon Depressions Forecast with Assimilation of Indian DWR Data Using WRF-3DVAR Analysis System, Pure Appl. Geophys., 170, 2329-2350, 10.1007/s00024-013-0648-z, 2013.

Rozenberg, G.: Optical characteristics of thick weakly absorbing scattering layers, Dokl. Akad. Nauk SSSR, 145, 775-777,1962.

Smith, T. M., Gao, J. D., Calhoun, K. M., Stensrud, D. J., Manross, K. L., Ortega, K. L., Fu, C. H., Kingfield, D. M., Elmore, K. L., Lakshmanan, V., and Riedel, C.: Examination of a Real-Time 3DVAR Analysis System in the Hazardous Weather Testbed, Weather Forecast., 29, 63-77, 10.1175/Waf-D-13-00044.1, 2014.

Srivastava, K., and Bhardwaj, R.: Analysis and very short range forecast of cyclone "AILA" with radar data assimilation with rapid intermittent cycle using ARPS 3DVAR and cloud analysis techniques, Meteorol. Atmos. Phys., 124, 97-111, 10.1007/s00703-014-0307-7, 2014.

Tegen, I., and Fung, I.: Contribution to the Atmospheric Mineral Aerosol Load from Land-Surface Modification, J. Geophys. Res.-Atmos., 100, 18707-18726, Doi 10.1029/95jd02051, 1995.

Tegen, I., Harrison, S. P., Kohfeld, K. E., Engelstaedter, S., and Werner, M.: Emission of soil dust aerosol: Anthropogenic contribution and future changes, Geochimica Et Cosmochimica Acta, 66, A766-A766, 2002.

Tegen, I., Werner, M., Harrison, S. P., and Kohfeld, K. E.: Relative importance of climate and land use in determining present and future global soil dust emission, Geophys. Res. Lett., 31, Artn L05105, 10.1029/2003gl019216, 2004.

Thompson, L. G., Davis, M. E., Mosleythompson, E., and Liu, K. B.: Pre-Incan Agricultural Activity Recorded in Dust Layers in 2 Tropical Ice Cores, Nature, 336, 763-765, Doi 10.1038/336763a0, 1988.

Toon, O. B., Mckay, C. P., Ackerman, T. P., and Santhanam, K.: Rapid Calculation of Radiative Heating Rates and Photodissociation Rates in Inhomogeneous Multiple-Scattering Atmospheres, J. Geophys. Res.-Atmos., 94, 16287-16301, Doi 10.1029/Jd094id13p16287, 1989.

Wallach, D. F. H., and Fischer, H.: Membrane aspects of the immune response. Report of a workshop held in Titisee, Schwarzwald, Germany, October 13–15, 1969, FEBS Lett. , 9, 129-135, 1970.

Atmospheric
Chemistry
and Physics
Discussions

Wang, M., Xu, B. Q., Zhao, H. B., Cao, J. J., Joswiak, D., Wu, G. J., and Lin, S. B.: The Influence of Dust on Quantitative Measurements of Black Carbon in Ice and Snow when Using a Thermal Optical Method, Aerosol Sci. Tech., 46, 60-69, 10.1080/02786826.2011.605815, 2012.

Wang, P., Che, H. Z., Zhang, X. C., Song, Q. L., Wang, Y. Q., Zhang, Z. H., Dai, X., and Yu, D. J.: Aerosol optical properties of regional background atmosphere in Northeast China, Atmos. Environ., 44, 4404-4412, 10.1016/j.atmosenv.2010.07.043, 2010a.

Wang, X., Huang, J. P., Ji, M. X., and Higuchi, K.: Variability of East Asia dust events and their long-term trend, Atmos. Environ., 42, 3156-3165, 10.1016/j.atmosenv.2007.07.046, 2008.

Wang, X., Huang, J. P., Zhang, R. D., Chen, B., and Bi, J. R.: Surface measurements of aerosol properties over northwest China during ARM China 2008 deployment, J. Geophys. Res.-Atmos., 115, Artn D00k27, 10.1029/2009jd013467, 2010b.

Wang, X., Doherty, S. J., and Huang, J. P.: Black carbon and other light-absorbing impurities in snow across Northern China, J. Geophys. Res.-Atmos., 118, 1471-1492, 10.1029/2012JD018291, 2013a.

Wang, X., Pu, W., Zhang, X. Y., Ren, Y., and Huang, J. P.: Water-soluble ions and trace elements in surface snow and their potential source regions across northeastern China, Atmos. Environ., 114, 57-65, 10.1016/j.atmosenv.2015.05.012, 2015.

Wang, X. G., Parrish, D., Kleist, D., and Whitaker, J.: GSI 3DVar-Based Ensemble-Variational Hybrid Data Assimilation for NCEP Global Forecast System: Single-Resolution Experiments, Mon. Weather. Rev., 141, 4098-4117, 10.1175/Mwr-D-12-00141.1, 2013b.

Wang, Z. W., Gallet, J. C., Pedersen, C. A., Zhang, X. S., Strom, J., and Ci, Z. J.: Elemental carbon in snow at Changbai Mountain, northeastern China: concentrations, scavenging ratios, and dry deposition velocities, Atmos. Chem. Phys., 14, 629-640, 10.5194/acp-14-629-2014, 2014.

Warren, S. G., and Wiscombe, W. J.: A Model for the Spectral Albedo of Snow .2. Snow Containing Atmospheric Aerosols, J. Atmos. Sci., 37, 2734-2745, Doi 10.1175/1520-0469(1980)037<2734:Amftsa>2.0.Co;2, 1980.

Warren, S. G.: Optical-Properties of Snow, Rev. Geophys., 20, 67-89, Doi 10.1029/Rg020i001p00067, 1982.

Wedepohl, K. H.: The Composition of the Continental-Crust, Geochimica Et Cosmochimica Acta, 59, 1217-1232, 1995.

Wright, P., Bergin, M., Dibb, J., Lefer, B., Domine, F., Carman, T., Carmagnola, C., Dumont, M., Courville, Z., Schaaf, C., and Wang, Z. S.: Comparing MODIS daily snow albedo to spectral albedo field measurements in Central Greenland, Remote Sens. Environ., 140, 118-129, 10.1016/j.rse.2013.08.044, 2014.

Wuttke, S., Seckmeyer, G., and Konig-Lang, G.: Measurements of spectral snow albedo at Neumayer, Antarctica, Ann. Geophys., 24, 7-21, 2006.

Xia, X. A., Chen, H. B., Wang, P. C., Zong, X. M., Qiu, J. H., and Gouloub, P.: Aerosol properties and their spatial and temporal variations over North China in spring 2001, Tellus B., 57, 28-39, 2005.

Xia, X. G., Li, Z. Q., Holben, B., Wang, P., Eck, T., Chen, H. B., Cribb, M., and Zhao, Y. X.: Aerosol optical properties and radiative effects in the Yangtze Delta region of China, J. Geophys. Res.-Atmos., 112, Artn D22s12, 10.1029/2007jd008859, 2007.

Xu, B. Q., Cao, J. J., Hansen, J., Yao, T. D., Joswia, D. R., Wang, N. L., Wu, G. J., Wang, M., Zhao, H. B., Yang, W., Liu, X. Q., and He, J. Q.: Black soot and the survival of Tibetan glaciers, Proc. Nat. Acad. Sci. U.S.A., 106, 22114-22118, 10.1073/pnas.0910444106, 2009.

Xu, B. Q., Cao, J. J., Joswiak, D. R., Liu, X. Q., Zhao, H. B., and He, J. Q.: Post-depositional enrichment of black soot in snow-pack and accelerated melting of Tibetan glaciers, Environ. Res. Lett. , 7, 10.1088/1748-9326/7/1/014022, 2012.

Yasunari, T. J., Bonasoni, P., Laj, P., Fujita, K., Vuillermoz, E., Marinoni, A., Cristofanelli, P., Duchi, R., Tartari, G., and Lau, K. M.: Estimated impact of black carbon deposition during pre-monsoon season from Nepal Climate Observatory - Pyramid data and snow albedo changes over Himalayan glaciers, Atmos. Chem. Phys., 10, 6603-6615, 10.5194/acp-10-6603-2010, 2010.

Ye, H., Zhang, R. D., Shi, J. S., Huang, J. P., Warren, S. G., and Fu, Q.: Black carbon in seasonal snow across northern Xinjiang in northwestern China, Environ. Res. Lett., 7, Artn 044002, 10.1088/1748-9326/7/4/044002, 2012.

Yesubabu, V., Srinivas, C. V., Hariprasad, K. B. R. R., and Baskaran, R.: A Study on the Impact of Observation Assimilation on the Numerical Simulation of Tropical Cyclones JAL and THANE Using 3DVAR, Pure Appl. Geophys., 171, 2023-2042, 10.1007/s00024-013-0741-3, 2014.

Zawadzka, O., Makuch, P., Markowicz, K. M., Zielinski, T., Petelski, T., Ulevicius, V., Strzalkowska, A., Rozwadowska, A., and Gutowska, D.: Studies of aerosol optical depth with the use of Microtops II sun photometers and MODIS detectors in coastal areas of the Baltic Sea, Acta Geophysica, 62, 400-422, 10.2478/s11600-013-0182-5, 2014.

Zege, E. P., Ivanov, A. P., and Katsev, I. L.: Image transfer through a scattering medium, Springer Verlag, 1991.

Zhang, R., Hegg, D. A., Huang, J., and Fu, Q.: Source attribution of insoluble light-absorbing particles in seasonal snow across northern China, Atmos. Chem. Phys., 13, 6091-6099, 10.5194/acp-13-6091-2013, 2013.

Zhang, R., Jing, J., Tao, J., Hsu, S. C., Wang, G., Cao, J., Lee, C. S. L., Zhu, L., Chen, Z., Zhao, Y., and Shen, Z.: Chemical characterization and source apportionment of PM2.5 in Beijing: seasonal perspective, Atmos. Chem. Phys. , 13, 7053-7074, 10.5194/acp-13-7053-2013, 2013.

Zhang, R. J., Arimoto, R., An, J. L., Yabuki, S., and Sun, J. H.: Ground observations of a strong dust storm in Beijing in March 2002, J. Geophys. Res.-Atmos., 110, 10.1029/2004jd004589, 2005.

Zhang, X. L., Wu, G. J., Kokhanovsky, A., Yao, T. D., and Tong D.: Spectral albedo parameterization for dirty snow with considering mirco-physicochemical properties of impurities - Part I: Theory and preliminary evaluation, 2016 (preparation).

Zhang, X. Y., Gong, S. L., Shen, Z. X., Mei, F. M., Xi, X. X., Liu, L. C., Zhou, Z. J., Wang, D., Wang, Y. Q., and Cheng, Y.: Characterization of soil dust aerosol in China and its transport and distribution during 2001 ACE-Asia: 1. Network observations, J. Geophys. Res.-Atmos., 108, Artn 4261, 10.1029/2002jd002632, 2003.

Zhao, C., Hu, Z., Qian, Y., Leung, L. R., Huang, J., Huang, M., Jin, J., Flanner, M. G., Zhang, R., Wang, H., Yan, H., Lu, Z., and Streets, D. G.: Simulating black carbon and dust and their radiative forcing in seasonal snow: a case study over North China with field campaign measurements, Atmos. Chem. Phys., 14, 11475-11491, 10.5194/acp-14-11475-2014, 2014.